

**DEVELOPMENT OF AN EFFECTIVE SINGLE LAYER MICRO-  
PERFORATED SOUND ABSORBER**

**ONURSAL ÖNEN**

**SEPTEMBER 2008**

DEVELOPMENT OF AN EFFECTIVE SINGLE LAYER MICRO-PERFORATED  
SOUND ABSORBER

A THESIS SUBMITTED TO  
THE GRADUATE SCHOOL OF NATURAL AND APPLIED SCIENCES  
OF  
MIDDLE EAST TECHNICAL UNIVERSITY

BY

ONURSAL ÖNEN

IN PARTIAL FULFILMENT OF THE REQUIREMENTS  
FOR  
THE DEGREE OF MASTER OF SCIENCE  
IN  
MECHANICAL ENGINEERING

SEPTEMBER 2008

Approval of the thesis:

**DEVELOPMENT OF AN EFFECTIVE SINGLE LAYER MICRO-PERFORATED  
SOUND ABSORBER**

submitted by **ONURSAL ÖNEN** in partial fulfillment of the requirements for the degree of **Master of Science in Mechanical Engineering Department, Middle East Technical University** by,

Prof. Dr. Canan ÖZGEN  
Dean, Graduate School of **Natural and Applied Sciences**

\_\_\_\_\_

Prof. Dr. S. Kemal İDER  
Head of Department, **Mechanical Engineering**

\_\_\_\_\_

Prof. Dr. Mehmet ÇALIŞKAN  
Supervisor, **Mechanical Engineering Dept., METU**

\_\_\_\_\_

**Examining Committee Members:**

Prof. Dr. Y. Samim ÜNLÜSOY  
Mechanical Engineering Dept., METU

\_\_\_\_\_

Prof. Dr. Mehmet ÇALIŞKAN  
Mechanical Engineering Dept., METU

\_\_\_\_\_

Prof. Dr. Yusuf ÖZYÖRÜK  
Aerospace Engineering Dept., METU

\_\_\_\_\_

Instr. Dr. Ender CİĞEROĞLU  
Mechanical Engineering Dept., METU

\_\_\_\_\_

Instr. Dr. Gökhan ÖZGEN  
Mechanical Engineering Dept., METU

\_\_\_\_\_

**Date:**

\_\_\_\_\_

**I hereby declare that all information in this document has been obtained and presented in accordance with academic rules and ethical conduct. I also declare that, as require by these rules and conduct, I have fully cited and referenced all material and results that are not original to this work.**

Name, Last Name :

Signature :

## **ABSTRACT**

### **DEVELOPMENT OF AN EFFECTIVE SINGLE LAYER MICRO-PERFORATED SOUND ABSORBER**

Önen, Onursal

M.Sc., Department of Mechanical Engineering

Supervisor: Prof. Dr. Mehmet Çalışkan

September 2008, 79 pages

Micro-perforated sound absorbers with sub-millimeter size holes can provide high absorption coefficients. Various types of micro-perforated absorbers are now available in literature for different applications. This thesis presents results of work on the development of an effective single layer micro-perforated sound absorber from the commercial composite material Parabeam<sup>®</sup> with micro diameter holes drilled on one side. Parabeam<sup>®</sup> is used as a structural material made from a fabric woven out of a E-glass yarn and consists of two decklayers bonded together by vertical piles in a sandwich structure with piles (thick fibers) woven into the decklayers. The thesis includes, the analytical model developed for prediction of absorption coefficients, finite element solution using commercial software MSC.ACTRAN and experimental results obtained from impedance tube measurements. Different absorption characteristics can be achieved by variations in hole diameter and hole spacing. Based on the developed models, an optimization is performed to obtain an efficient absorber configuration. It has been anticipated that several different and interesting applications can be deduced by combining structural and sound absorption properties of this new micro-perforated absorber along with conventional fibrous absorbers.

Keywords: Micro-perforated Absorber, Acoustic Impedance, Absorption Coefficient,  
Finite Element Method

## ÖZ

### ETKİN BİR TEK KATMANLI MİKRO DELİKLİ SES YUTUCU GELİŞTİRİLMESİ

Önen, Onursal

Yüksek Lisans, Makina Mühendisliği Bölümü

Tez Yöneticisi: Prof. Dr. Mehmet Çalışkan

Eylül 2008, 79 Sayfa

Mikro delikli ses yutucu malzemeler bir milimetreden küçük çaplı deliklerde yüksek ses yutma katsayısı değerleri sağlayabilir. Çeşitli türde mikro delikli ses yutucular üzerine yapılan çalışmalar, farklı uygulama alanları kapsayacak şekilde literatürde yer almaktadır. Bu tez çalışması, ticari kompozit malzeme Parabeam<sup>®</sup>, in bir yüzüne küçük çaplı delikler delerek bu malzemedan etkin bir tek katmanlı mikro delikli ses yutucu geliştirilmesi için yapılan çalışmaların sonuçlarını içermektedir. Parabeam<sup>®</sup>, E tipi cam elyaftan oluşan iki plaka ve bu iki plakayı birleştiren örülmüş kalın ipliklerden oluşan yapısal bir malzemedir. Tez çalışması, ses yutma katsayıları tahmini için geliştirilmiş analitik model, ticari yazılım MSC.ACTRAN kullanarak yapılan akustik sonlu elemanlar çözümü ve çeli tüpü kullanılarak elde edilen deneysel sonuçlarını içermektedir. Değişik delik çapları ve delikler arası uzaklıklar ile çeşitli farklı ses yutma karakterleri elde edilebilmektedir. Geliştirilen modeller yardımıyla etkin bir ses yutucu yapısı elde edilmesi için bir optimizasyon gerçekleştirilmiştir. Bu yeni mikro delikli ses yutucunun yapısal ve ses yutma özelliklerini birleştirerek geleneksel lifli yapıdaki ses yutucu malzemeler ile birlikte çeşitli farklı ve ilginç uygulamalar mümkün görülmektedir.

Anahtar kelimeler: Mikro Delikli Ses Yutucu, Akustik Çeli, Ses Yutma Katsayısı,  
Sonlu ElemanlarYöntemi.

**To My Family**

## **ACKNOWLEDGEMENTS**

The author wishes to express his deepest gratitude to his supervisor Prof. Dr. Mehmet Çalışkan for guidance, advice, criticism, encouragements and insight throughout the research.

Aydın Kuntay of BIAS Inc. of Turkey, Jonathan Jacqmot of FFT Technologies Pty. Ltd., Jaap Jan Kleef of Parabeam<sup>®</sup> 3D Glass Fabrics B.V., Eyüp Turhan of METU, Mechanical Engineering Department and Wael Elwali are gratefully acknowledged for their help and assistance.

The author would also like thank his family for their invaluable support and encouragement throughout the research.

# TABLE OF CONTENTS

ABSTRACT .....	iv
ÖZ .....	vi
ACKNOWLEDGEMENTS .....	ix
TABLE OF CONTENTS .....	x
LIST OF FIGURES .....	xii
LIST OF SYMBOLS .....	xiv
CHAPTERS	
1. INTRODUCTION .....	1
1.1 General .....	1
1.2 Parabeam <sup>®</sup> .....	3
1.3 Scope and Objective of the Thesis .....	5
2. LITERATURE REVIEW .....	8
2.1 Micro-perforation Theory .....	8
2.2 Inner Structure .....	11
2.3 Finite Element Methods on Micro-perforated Absorbers .....	14
2.4 Applications of Micro-perforated Absorbers .....	15
2.5 Sound Transmission and Radiation .....	18
3. THEORETICAL DEVELOPMENT .....	20
3.1 Introduction .....	20
3.2 Acoustic Impedance .....	20
3.3 Transfer Matrix Method .....	21

3.4 Impedance of Micro-Perforated Layer.....	25
3.5 Impedance of Porous Layer .....	31
3.6 Impedance of Air Cavity.....	32
3.7 Determination of Absorption Coefficient .....	33
4. ANALYTICAL MODELING.....	34
4.1 Overview of Analytical Model.....	34
4.2 Results .....	35
5. FINITE ELEMENT MODELING .....	40
5.1 Finite Element Modeling .....	40
5.2 Determination of the Acoustic Impedance at the Top of the Fibrous Layer of Parabeam <sup>®</sup> .....	43
5.3 Results of Predictions of Normal Incidence Absorption Coefficients from Finite Element Model.....	45
6. EXPERIMENTAL RESULTS.....	48
6.1 Measurement Set-up.....	48
6.2 Results of Impedance Tube Measurements.....	52
7. COMPARISON OF RESULTS AND OPTIMIZATION.....	56
7.1 Comparison of Results .....	56
7.2 Optimization.....	59
8. DISCUSSIONS AND CONCLUSIONS .....	62
REFERENCES.....	66
APPENDICES	
A. MATLAB <sup>®</sup> CODE OF THE ANALYTICAL MODEL .....	72
B. FINITE ELEMENT THEORY OF MSC.ACTRAN MODAL BASIS .....	75

## LIST OF FIGURES

### FIGURES

Figure 1. Side view of Parabeam <sup>®</sup> with eight-shaped fibers.....	3
Figure 2. Incident and reflected wave at the boundary $x=0$ .....	23
Figure 3. Predicted normal incidence absorption coefficients for Sample 1 obtained from analytical model .....	36
Figure 4. Predicted normal incidence absorption coefficients for Sample 2 obtained from analytical model .....	37
Figure 5. Predicted normal incidence absorption coefficients for Sample 3 obtained from analytical model .....	37
Figure 6. Predicted normal incidence absorption coefficients for Sample 4 obtained from analytical model .....	38
Figure 7. A general view of finite element model .....	40
Figure 8. An illustration of model built for determination of acoustic impedance at the top of the fibrous layer .....	44
Figure 9. Real and imaginary parts of acoustic impedance at the top of fibrous layer obtained from finite element modeling .....	44
Figure 10. Predicted normal incidence absorption coefficients for Sample 1 obtained from finite element model.....	45
Figure 11. Predicted normal incidence absorption coefficients for Sample 2 obtained from finite element model.....	46
Figure 12. Predicted normal incidence absorption coefficients for Sample 3 obtained from finite element model.....	46
Figure 13. Predicted normal incidence absorption coefficients for Sample 4 obtained from finite element model.....	47
Figure 14. A schematic of the standing wave impedance tube set-up .....	49

Figure 15. The experimental set-up used in impedance tube measurements.....	52
Figure 16. The samples used in measurements.....	53
Figure 17. Measured normal incidence absorption coefficients for Sample 1.....	53
Figure 18. Measured normal incidence absorption coefficients for Sample 2.....	54
Figure 19. Measured normal incidence absorption coefficients for Sample 3.....	54
Figure 20. Measured normal incidence absorption coefficients for Sample 4.....	55
Figure 21. Results of predicted and measured normal incidence absorption coefficients for Sample 1 .....	57
Figure 22. Results of predicted and measured normal incidence absorption coefficients for Sample 2 .....	57
Figure 23. Results of predicted and measured normal incidence absorption coefficients for Sample 3 .....	58
Figure 24. Results of predicted and measured normal incidence absorption coefficients for Sample 4 .....	58
Figure 25. Results of predicted and measured normal incidence absorption coefficients for the optimized absorber.....	60

## LIST OF SYMBOLS

$p$	Pressure (Pa)
$v$	Particle velocity (m/s)
$S$	Surface area (m <sup>2</sup> )
$Z$	Acoustic impedance (kg/m <sup>4</sup> s)
$X$	Acoustic resistance (kg/m <sup>4</sup> s)
$j$	Unit imaginary number ( $=\sqrt{-1}$ )
$M$	Mass reactance (kg/m <sup>4</sup> s)
$A$	Complex constant
$\omega$	Angular frequency (rad/s)
$c_0$	Speed of sound in air (m/s)
$\kappa$	Attenuation constant
$\gamma$	Propagation constant
$\beta$	Phase constant
$Z_l$	Specific acoustic impedance of a layer (kg/m <sup>2</sup> s)
$l$	Thickness of an arbitrary absorber layer (m)
$P_i$	Amplitude of pressure of incident wave (Pa)
$P_r$	Amplitude of pressure of reflected wave (Pa)
$Z(x)$	Specific acoustic impedance at point $x$ (kg/m <sup>2</sup> s)
$p(x)$	Pressure at point $x$ (Pa)
$v(x)$	Particle velocity at point $x$ (m)
$Z_2$	Specific acoustic impedance at the top of layer $l$ (kg/m <sup>2</sup> s)
$\theta$	Angle of incidence
$\rho$	Density of air (kg/m <sup>3</sup> )
$\bar{\nabla}$	Gradient operator
$\bar{v}$	Vectorial particle velocity (m/s)
$\mu$	Dynamic viscosity of air (Pa.s)

$\bar{g}$	Gravitational acceleration ( $\text{m/s}^2$ )
$T$	Stress tensor
$r$	Radial distance inside a hole (m)
$s$	Perforate constant 1
$J_0$	Bessel's equation of type 1, order 0
$R_h$	Radius of a hole (m)
$J_1$	Bessel's equation of type 1, order 1
$h$	Perforate constant 2
$Z_{hole}$	Specific Acoustic impedance of a hole ( $\text{kg/m}^2\text{s}$ )
$Z_{hole,m}$	Corrected Specific Acoustic impedance of a hole ( $\text{kg/m}^2\text{s}$ )
$Z_{perf}$	Specific Acoustic impedance of a perforated layer ( $\text{kg/m}^2\text{s}$ )
$\varepsilon$	Perforation ratio
$a$	Hole pitch (m)
$Z_{top}$	Specific Acoustic impedance at the top of a perforated layer ( $\text{kg/m}^2\text{s}$ )
$Z_{po}$	Characteristic acoustic impedance of a porous layer ( $\text{kg/m}^2\text{s}$ )
$f$	Frequency (Hz)
$\rho_0$	Density of air under standard conditions ( $\text{kg/m}^3$ )
$R_f$	Flow resistivity (Pa/m)
$k$	Wave number (1/m)
$\gamma_{po}$	Propagation constant in a porous layer
$Z_{porous}$	Specific acoustic impedance of a porous layer ( $\text{kg/m}^2\text{s}$ )
$t_{po}$	Thickness of a porous layer (m)
$Z_a$	Characteristic acoustic impedance of air ( $\text{kg/m}^2\text{s}$ )
$\gamma_a$	Propagation constant in an air
$k_a$	Wave number in air (1/m)
$t_{po}$	Thickness of an air layer (m)
$R$	Reflection coefficient
$Z_{tot}$	Total specific acoustic impedance at the top of an absorber assembly ( $\text{kg/m}^2\text{s}$ )
$\alpha$	Normal incidence absorption coefficient
$Re$	Real part of a complex number
$Im$	Imaginary part of a complex number
$P_{max}$	Maximum pressure amplitude in impedance tube (Pa)

$P_{max}$	Minimum pressure amplitude in impedance tube (Pa)
$SWR$	Standing wave ratio
$\zeta$	Phase angle (rad)
$z_{min}$	Distance between the sample and position of microphone where first minimum pressure is read in impedance tube
$f_u$	Upper frequency limit of measurements in impedance tube

# CHAPTER 1

## INTRODUCTION

### 1.1 General

Sound absorbing materials have been extensively used in various acoustical applications for a very long time both indoors and outdoors. Sound absorbers are being used not only in passive noise control practice but also in room acoustics. For control of unwanted sound, namely noise, or for acoustic fields inside enclosed spaces, acoustical energy should somehow be removed from the medium. Sound absorbing materials are typically designed, optimized and used for controlling noise or for obtaining better acoustical characteristics in residential locations, offices, industrial plants, theaters, concert halls or any kind of space where noise or sound is an important aspect.

Absorption characteristics of any material should be known for acoustical design. With the knowledge of frequency dependent acoustical properties of absorbers, the characteristics of noise and acoustical field in that environment can be estimated. Considerable effort has been devoted on the prediction of absorption characteristics of different absorbing materials with emphasis on developing quick, accurate and inexpensive prediction tools.

Fibrous and porous absorbers are the most common sound absorbing materials that are being used in passive noise control applications when high level of absorption is desired. However, such kinds of absorbers have some limitations. Very thick absorbing material is required when high absorption at low frequencies is desired.

This may constitute problems in terms of space and cost. Also, fibrous absorbing materials are known as dangerous for health which limits use of these kinds of materials in hospitals and other environments, where hygiene is a critical issue. Also, fibrous materials are not resistant to moist, oil and dust. A surface finish is naturally required to overcome these problems and to provide aesthetic qualities.

Recently, there has been an increasing effort on developing cleaner and more health-friendly absorbing materials. Micro-perforated absorbers are becoming popular because of being clean, health-friendly and flexible in design. Variety of materials can be used, resulting in high sound absorption coefficients at low frequencies with relatively low thicknesses compared to porous and fibrous absorbers. Perforated absorbers have been used for some time with large hole diameters (millimeter or centimeter size) and high perforation ratios (ratio of open area to the total area) in exterior facings combined with other sound absorption materials like fibrous and porous absorbers for sound absorption. However, with such large hole diameters and perforation ratios, perforated absorbers are not effective sound absorbers alone, mainly because they lack sufficient acoustic resistance. Micro-perforated absorbers with small hole diameters and low perforation ratios show good properties by means of relatively high acoustic resistance and mass reactance resulting in good sound absorption performance. Micro-perforated sound absorbers are basically of metal, plastic or wooden panels (or membranes) with very small holes drilled on panels and an air gap between the perforated panel and the rigid wall or backing. Effective absorption covering a bandwidth of 5 to 6 octaves can be obtained by appropriate adjustment of parameters in a single layer micro-perforated absorber.

For prediction of absorption characteristics of micro-perforated absorbers, various models have been developed and investigated in detail in the existing literature. Acoustic properties of micro-perforated absorbers with different perforation characteristics by variation of diameter of holes, hole spacing, profile of holes and with different inner structures including fibrous/porous absorbers, honeycomb structures, air spaces and some other complex structures exist in literature. Parabeam<sup>®</sup> is anticipated to be a good candidate for an effective micro-perforated absorber.

## 1.2 Parabeam®

Parabeam® is a 3D glass fabric, which is woven out of E-glass yarn and consists of two decklayers bonded together by vertical piles in a sandwich structure [1]. These piles (or namely thick fibers) are woven into the decklayers thus forming an integral sandwich structure. Parabeam is a commercial composite material that is produced by Parabeam® 3D Glass Fabrics B.V.. The curing process of Parabeam® involves impregnation of a thermoset resin to the woven. When woven fabric is impregnated with resin, the fabric absorbs the resin and due to the capillary forces of the piles, the fabric rises to the preset height. In this one step process, a lightweight and strong sandwich laminate is formed. The cured fibers in the mid layer is distributed and oriented inside the layer in such a way to form that looks like an eight shaped structure, which is illustrated in Figure 1 [1].

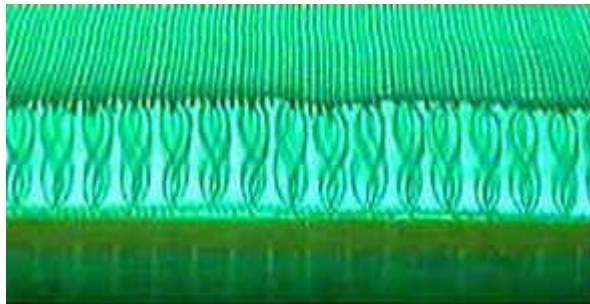


Figure 1. Side view of Parabeam® with eight shaped fibers [1]

There are two main product branches of Parabeam®: ParaGlass and ParaTank. ParaGlass is the type investigated in this thesis. It is available in the thicknesses of 3, 5, 8, 10, 12, 15, 18 and 22 mm. ParaTank is used in pressurized vessels with a special pile configuration and is not investigated in this thesis. In this specific work, ParaGlass 18 is the type of material chosen for design of a micro-perforated sound absorber. The thickness of the fibrous layer is 18 mm and the thickness of the micro-

perforated layer is 1mm. Mechanical properties of ParaGlass 18 are given in Table 1 [1].

Main advantages of Parabeam<sup>®</sup> can be listed compared with common sandwich structures as: low resin absorption, integral sandwich structure, fast and easy one-step processing procedure, good strength to weight ratio, no delamination, no corrosion or rotting, ease of reparability and drapeability. Parabeam can be used with a wide variety of thermoset resins like polyester, epoxy, phenolic and vinlyster resins.

Parabeam<sup>®</sup> can be shaped and elaborated during production process to any possible desired geometry and shape. Also, Parabeam<sup>®</sup> can be constructed with different attachments, connections, built-in fasteners and edge closings. Also during the curing process, any other material compatible with E-Glass and the thermoset resin can be assembled to Parabeam<sup>®</sup> either for enhancing mechanical properties or just as a surface finish by using a material like wood, foam, steel and aluminum [1].

Table 1. Mechanical Properties of ParaGlass 18 (without perforations) [1]

Mass - Fabric (kg/m <sup>2</sup> )	1,72
Mass - Laminate (kg/m <sup>2</sup> )	3,61
Compressive Strength (N/mm <sup>2</sup> )	0,9
Shear Strength (N/mm <sup>2</sup> )	0,1
Shear Modulus (N/mm <sup>2</sup> )	1,8
Bending Stiffness (Nm <sup>2</sup> )	55,9

Parabeam<sup>®</sup> is used for many applications in marine industry (bulkheads, deck, hatches, doors, interior and floor panels, furniture, hulls, superstructures, ceiling panels, ducts), railway (node cones, interior panels / floors / walls / ceilings, sanitary units), automotive industry (air-deflectors, hardtops, skirts, spoilers, top sleepers, floor panels, roofing, side walls, trailers, caravans), and in building and construction

business (domes, radomes, kiosks, amusement parks, bridges, claddings, industrial roofing and flooring, tooling, wet-units, billboards, utility cabins, partitioning walls, exhibition panels and furniture) [1]. With all the listed applications, addition of a sound absorbing property with simply drilling micro size holes on Parabeam<sup>®</sup> seems possible without altering the mechanical properties too much.

### **1.3 Scope and Objective of the Thesis**

In this particular study, it is aimed to develop an effective single layer micro-perforated absorber from the commercial composite material Parabeam<sup>®</sup> with micro diameter holes drilled on one side.

Analytical modeling is the first tool considered for prediction of absorption characteristics. Analytical modeling offers fast and easy prediction in most of the engineering problems with the help of modern computing tools if the model developed can properly represent the physics of the problem. In this work, analytical model basically relies on the developed models available in literature which are usually verified by experimentations in several different applications and configurations. In this process, It is aimed to develop an accurate prediction tool not only for the absorber to be built from Parabeam<sup>®</sup>, but also a general tool to predict absorption characteristics of different multi layer absorber configurations and assemblies. With the developed analytical model, normal incidence absorption coefficients of absorber configurations consisting of micro-perforated, porous or fibrous absorber and Parabeam<sup>®</sup> layers with air gaps in between these layers can be predicted with clearly identifying intermediate parameters like acoustic resistance, mass reactance and reflection coefficient. In the analytical model developed, prediction ability is limited to common materials and configurations that are already investigated in literature.

Finite element modeling is another important approach to acoustical problems with complex and unusual geometries. Finite element modeling can be counted as an essential tool for prediction, although it is time consuming and costly compared with analytical models. With the finite element model built, even for a complex geometry

and structure, it is possible to predict resulting acoustical properties that can not be evaluated by any analytical model. In finite element modeling it is possible to model acoustical and structural interaction with defining proper boundary conditions and interfaces. Since there is no existing work in literature for modeling the layer consisting thick fibers and air gap between the two plates of Parabeam<sup>®</sup>, it is decided to use finite element modeling to predict the absorption coefficient including effect of the thick fibers inside the cavity. Also acoustical properties of this layer for use in the developed analytical model are also obtained from the finite element model.

Experiments are conducted using a single microphone impedance tube for verification of the results obtained from the two prediction tools: analytical and finite element modeling. Four micro-perforated absorber samples produced from Parabeam<sup>®</sup> are used in experiments to validate the accuracy of the predictions with different hole diameters and different hole spacing (resulting in different perforation ratios). The measurements are made in accordance with the related standards for impedance tube measurements. Results obtained from measurements show good agreement with the results obtained from analytical and finite element models. With the good agreement shown, it can be concluded that the analytical model developed alongside with finite element model can be used as an effective tool for designing micro-perforated absorbers from Parabeam<sup>®</sup>.

The next chapter includes a brief summary of existing work in literature under five main topics including main subjects of this study and applications.

Chapter 3 presents derivation of analytical expressions that are used throughout this study, to develop the analytical model and to interpret the physics underlying the subject. A complete theory is outlined from the concept of acoustic impedance to the prediction of normal incidence absorption coefficients.

Chapter 4 presents development of the analytical model and results obtained from this model using the relations given in Chapter 3. The MATLAB<sup>®</sup> code written for the prediction of absorption coefficients is explained in detail and results obtained from the code is shown.

Detailed information on the finite element model is explained in Chapter 5. Development of the model and the solution procedure are briefly explained and results obtained are illustrated.

In Chapter 6, theory underlying the impedance tube measurements, details of the measurement setup and results of the measurements are given.

A comparison of the results obtained from analytical model, finite element model and impedance tube measurements is presented in Chapter 7. Also, the optimization procedure and its outcome are given in this chapter.

Finally, in Chapter 8, discussions and conclusions on the subject are summarized. Recommendations for possible future work are also presented within this chapter.

## **CHAPTER 2**

### **LITERATURE REVIEW**

In this chapter, summary of the literature survey is given starting with the theory of micro-perforated absorbers. Works on various inner structures and inner structure materials, applications, finite element methods and radiation from and transmission through the micro-perforated absorbers are also discussed in detail.

#### **2.1 Micro-perforation Theory**

Maa has firstly proposed that effective sound absorbers can be developed by reducing the hole diameters to sub millimeter size [2]. It is proposed that, perforated absorbers with sub millimeter holes can result in an effective and wideband panel absorber covering 5 to 6 octaves. In Maa's work, starting with impedance of a single hole and using electro-acoustic analogy, normal incidence absorption coefficients of micro-perforated absorber are predicted. It has been shown that predicted absorption coefficient values and experimental results are in good agreement. Maa also proposed a design methodology for such kinds of absorbers [3]. Through this method, absorbers can be designed for desired absorption bandwidth and resonance frequency by properly adjusting design parameters with the help of charts and simplified equations.

Stinson and Shaw are also among first who worked on micro-perforations [4]. They worked on calculation of acoustic impedance of small, circular orifices starting from orifice formulation of Crandall [5]. The equations for resistance and inertance they had developed, however, are applicable to micro-perforated absorber in a specified

range. For verification of the theory, they performed impedance tube measurements using 5 different samples. Results are fairly good compared with values obtained from theoretical formulation.

Another important work on prediction of random incidence absorption coefficients is performed by Zou *et al.* [6]. In this work, a method named as ‘impedance transfer method’ (ITM) is used in addition to electro-acoustic analogy and equivalent circuit approach, for correcting normalized normal acoustic impedance of a single cavity. In this approach, the effect of directional properties of sound propagation inside the air gap has taken into consideration. Reverberation chamber measurements show that by using ITM, accuracy of predictions is notably increased for random incidence.

Chongyun and Quibai also proposed a theoretical method for predicting absorption coefficients of multi layer absorbers composed of micro-perforated plates, air spaces and porous materials [7]. Absorption coefficients of absorbers composed of perforated plates, airspaces and porous materials are calculated using an iterative method. For the three proposed configurations, predictions are validated by experiments and results show good agreement with the calculated values.

Another important study is conducted by Lee and Chen [8], in which existing literature is summarized and a prediction tool is built for micro-perforated absorber assemblies by utilizing acoustic transmission analysis. The model developed includes the micro perforation model of Maa [2] and porous absorber model of Delany and Bazley [9]. Effects of various configurations are investigated with different perforation ratios of micro perforations, porous absorbers and with different arrangements of the same perforated plates theoretically.

Kang and Fuchs worked on determination of absorption characteristics of open weave textiles and micro-perforated membranes [10]. They also used Maa’s [2] electro-acoustic analogy for developing an analytical model with appropriate corrections for predicting absorption coefficient for both normal and random incidence, for single and double layer absorbers. Normal incidence predictions are

validated using an impedance tube system whereas random incidence predictions are checked by reverberation chamber measurements separately.

Takahashi used a different approach to predict random incidence absorption characteristics of micro-perforated absorber systems [11]. The problem is treated as a wave scattering problem from a boundary surface with a correction introduced for impedance discontinuities at the surface boundary. An analytical model is proposed using admittance concept, also taking effects of edge diffractions and panel vibration into account. Results derived from the analytical model had been tried to be validated by experimentation. However, the agreement between results is fairly good. Another methodology for prediction of reverberation chamber absorption characteristics of micro-perforated absorbers is presented by Sakagami *et al.* [12]. A theoretical model is developed using existing models available in literature considering sound incidence from both sides in double-leaf perforated absorber and edge effects are also considered.

Another approach, based on modal analysis is made by Lee *et al.* [13]. In their work, the effect of panel vibration is included in the absorption mechanism by modal analysis of the classic plate equation coupled with the acoustic wave equation. Their work shows that, the absorption peaks due to vibration of the perforated panel can widen the absorption bandwidth of the absorber. They also stated that, higher modes of panel vibration do not significantly affect absorption performance and the effect of structural damping can improve absorption performance at frequencies other than structural resonance frequencies. Lee *et al.* further worked on an electrical circuit model based on Maa's analogy [2] investigating effects of Helmholtz resonance and panel resonance in parallel on micro-perforated absorbers [14]. They also showed that proper use of panel resonance and Helmholtz resonance can widen the absorption bandwidth.

Sakagami *et al.* also worked on the effects of panel vibration and density of the light weight perforated panel on the absorption coefficient of perforated absorber [15]. Sakagami introduces the effect of panel vibration into the classical electro-acoustic model [2] by addition of a term related with panel surface density to the impedance

expression. It is shown that, the effect of changing panel density has only an effect on the resonance peaks. It is also noted that, the panel vibration lowers the peak absorption values by 10 %.

Takahashi and Tanaka also present a method of theoretical treatment of acoustical coupling due to flexural vibration of perforated plates and plates of porous elastic materials [16]. The model is developed using the flow continuity at the plate surface in a mean sense and air-solid interaction. For the specific case investigated with decreasing perforation ratios, it is seen that the effect of plate vibration on absorption characteristics is enhanced with this decrease. Micro-perforated plates and porous elastic materials are treated with classical thin-plate theory and a theoretical procedure is developed using Helmholtz integral formulation.

Another approach for prediction of absorption coefficients of multi-layer perforated absorber systems is introduced by Leea and Kwon, by applying transfer matrix method [17]. The absorption coefficient of the perforated absorber is estimated from the overall transfer matrix obtained by multiplying unit transfer matrices for perforated panels or airspaces.

## **2.2 Inner Structure**

In the existing literature, empirical equations used for prediction of acoustic properties of fibrous and porous materials are mainly based on equations of Delany and Bazley [9]. Even if these equations are frequently used, it is known that they provide unphysical predictions and result in large errors for low frequencies. Alard developed more accurate empirical equations for modeling sound propagation in fibrous materials [18] with an improved model based on Delany and Bazley's equations. The new equations are suggested as more effective especially at low frequencies. The expressions are derived using the general frequency dependence of the viscous forces in porous materials with transposition carried out to predict the dynamic bulk modulus of air. Through this work, it is found that sound propagation in fibrous materials depend mainly on fiber diameter and density of the material.

Poroelastic plates and thin films are frequently used in inner structures of multi-layer absorbers. Horoshenkov and Sakagami developed a solution procedure for the acoustic field reflected from a finite, thin, poroelastic plate in a rigid baffle with simply supported edges [19]. The solution procedure relies on the Helmholtz integral equation formulation. The effect of air gap between the plate and the rigid wall is also considered. An analytical model is developed to predict the average value of acoustic impedance and absorption coefficient by using structural velocity of the poroelastic plate and acoustic pressure.

Sugie *et al.* worked on absorption characteristics of a fibrous material covered with a perforated facing and an impermeable film. They investigated the effect of the interactions between them based on Bolt's model [20]. In their work, the end corrections for the holes of the perforated membrane are determined experimentally with samples of different perforation ratios and macro holes of 10 mm in diameter. Their work mainly focused on a thin perforated layer (approximately 1 mm thick) with a high perforation ratio and relatively large diameter holes. Such facings are widely used in outdoor noise barriers. The prediction methodology mainly includes, combined vibration of the perforated facing and the film and the increase in acoustic resistance of the absorber by addition of the film and the perforated facing. The predictions and measurements agreed well in normal incidence, except in cases where the film was pinched by the perforated facing and fibrous material.

Lee *et al.* have performed experimental work on acoustic impedance of perforations in contact with fibrous materials on samples by varying the density of fibrous material used, hole diameters and perforation ratios of the perforated layer [21]. In their work, a modified impedance tube system with four microphones is used. The complex characteristic impedance and wave number of the fibrous materials are also determined experimentally in the four-microphone impedance tube other than using empirical models. Effects of different interfaces between perforated layer, fibrous material and air are experimentally determined by measurement of acoustic impedance.

Hong *et al.* conducted a research on developing composite porous sound absorber using recycled rubber particles with variable particle diameters [22]. It is shown that, impedance matching design of structure using a perforated cover, combination of damping effect with conventional viscothermal mechanisms and the effect of cavity resonance makes up a good absorber. Through the acoustic transmission analysis, acoustic absorption coefficients for composite absorber are evaluated and contribution of recycled rubber on low-frequency sound absorption is confirmed.

Another absorber configuration was proposed by Atalla *et al.* including a macro-perforated porous absorber with square holes drilled inside the mineral wool with holes either left unfilled or filled by other kinds of absorbers to improve the absorption performance [23]. The absorption coefficient of non-homogeneous porous layers has been predicted from a 3-D numerical finite element model and an experimental validation has been presented. Bécot *et al.* also worked on same type of ‘double porosity’ absorber [24] both theoretically using a model based on Delany and Bazley’s [8] and experimentally. With randomly positioned holes with different diameters, theoretical and experimental results came out to be very much similar.

Permeable membranes are occasionally used in absorber assemblies. An investigation on double leaf membrane absorber is made by Sakagami *et al.* that include a double layer absorber with a permeable membrane at the sound-incident side [25]. The most important conclusion is that, with the proposed configuration low frequency absorption is independent of the air cavity in-between. Takahashi *et al.* also worked on permeable membrane theory for prediction of absorption characteristics of permeable membranes in absorber assemblies [26]. Especially at mid and high frequencies, developed analytical model is in correspondence with measurements.

Another interesting inner structure is proposed by Godbold *et al.* with concentric fins placed inside a cavity [27]. Authors propose concentric fins, which are manufactured by a special manufacturing process called Selective Laser Sintering (SLS), also called as Solid Freeform Fabrication or Rapid Prototyping. Effects of concentric fins are compared with micro-perforations installed inside the same cavity in a similar

way. It is shown that concentric fins have similar effects like micro perforations by showing adequate acoustic resistance. These fins result in a wider frequency band for absorption and have better absorption coefficient values compared with the micro-perforated absorber.

### **2.3 Finite Element Methods on Micro-perforated Absorbers**

Finite element method is another major approach to acoustic problems in the low frequency range. Chen *et al.* used a finite element procedure, derived by Galerkin residual method and Helmholtz wave propagation equation for predicting absorption characteristics of perforated plates and porous material layers with various shapes placed inside the air cavity of the micro-perforated absorber [28]. In this work, four surface shapes of commercially available porous materials: triangle, semicircle, convex rectangle and plate are used. They studied on prediction of sound absorption coefficients by using these various shaped porous materials with different porosities and flow resistivity values. For the verification of predicted absorption characteristics, a two-microphone impedance tube setup is used.

Lee and Chen further developed their work on finite element method by analyzing multiple layer micro-perforated absorbers again with different perforated surface shapes inlaid with porous absorbers [29]. In this work, apart from conventional finite elements analysis, they simulate perforated plates by introducing appropriate equivalent boundary conditions depending on design parameters. Introduction of boundary layers to the model results in reducing total degrees of freedom in the model. They also designed, manufactured and tested a multi-layer absorber with a novel, optimized profile. One of the important conclusions derived is that more porous material in front of perforated plate enhances absorption at higher frequency bands while more porous material behind the perforated plate enhance absorption at lower frequency bands.

Panteghini *et al.* also worked on finite element solution of micro-perforated absorbers [30]. They worked on an absorber configuration with a glass wool layer backed by a rigid wall, air cavity and a micro-perforated layer for handling of low

frequency resonances in medium sized rooms. In the paper, results of finite element solution using full-scale absorber model and a micro scale model of the same absorber containing a single hole is obtained. Also, an analytical model is developed and impedance-tube measurements are performed for verification. Results show good agreement at mid frequencies, but fairly good agreement at low frequencies. Finite element solution is performed by direct analysis other than modal analysis. An important note is that, results of full-scale finite element solution and the finite element solution of single cell are exactly the same.

## **2.4 Applications of Micro-perforated Absorbers**

Chiu *et al.* worked on the design of a single layer micro-perforated sound absorber by use of graphic analysis and computer aided numerical-assessment [31]. The absorber developed is composed of a micro-perforated plate, a glass fiber layer and an air gap. The absorber was designed for a particular noise control application inside a constrained manufacturing system, where noise around 500 Hz dominates the whole noise. Absorption characteristics of the micro-perforated sound absorber are determined using matrix transfer method. The objective function for optimization is set up by dividing the absorption coefficient by the glass wool thickness with a prerequisite maximum thickness of 20 cm. The objective function is modified to obtain a high absorption value at 500 Hz and minimum fiber usage. As a result of this work, an optimized absorber is designed.

Another computer-aided design procedure is developed by Shen and Wang [32]. A design tool using impedance transfer method (ITM) [6] and a genetic algorithm enabling an iterative design of micro-perforated absorbers is introduced. The tool itself outputs all of the parameters required for the micro-perforated absorber to match the desired absorption characteristic input to genetic algorithm.

Sometimes, micro-perforated sound absorbers need to be cleaned frequently, because holes may be filled with dust, dirt, etc. Kang and Fuchs propose water for cleaning micro-perforated absorbers and they worked on the effect of water-films on absorption characteristics of these absorbers [33]. By experiments, they conclude that

water films generally decrease absorption coefficients especially when the absorber and water film is horizontal. Vertical films cause less decrease. They also found that thin films, with a thickness, say 1mm, can effectively clean absorber and do not have much effect on absorption characteristics. Also, the noise caused by the flow of water over the perforated plate is acceptable in most silencer applications.

In some applications, backing the perforated sheet or plate with a rigid wall may not always be possible. For such cases, Sakagami *et al.* made a numerical study on a double leaf micro-perforated absorber [34] using a modified version of Maa's analogy [2]. They also compared their results with double leaf permeable membranes with the same configurations. The resulting absorber has the characteristics of a typical micro-perforated absorber (with rigid backing wall) at medium and high frequencies and those low frequency absorption capabilities of double leaf permeable membrane absorber. As a concluding remark, authors suggest surface resistance values for broadband and high levels of absorption. Further on double leaf micro-perforated panel absorbers, Sakagami *et al.* revised the theory on micro-perforated absorbers investigating the difference in electro-acoustical analogy proposed by Maa [2] and the theory they have introduced in their paper [35] using a Helmholtz integral formulation. The results show that electro acoustical analogy tends to exaggerate the resonance behavior of the air cavity, thus increasing the absorption coefficients around the resonance frequency.

Another solution to poor performance of thin perforated layers is proposed by Yairi *et al.* [37]. For supporting thin layers of double leaf perforated absorber to avoid excessive panel vibration with incident sound, partly or fully filling the air cavity is suggested. Best absorption performance is obtained by fully filling the cavity with honeycomb structure. Toyoda *et al.* also worked on honeycomb backed microperforated absorbers backed by a rigid wall [38]. A perforated system for reducing the radiated sound from a plate at arbitrary frequencies is applied to three-dimensional problem. Plates are assumed to be supported in a duct of a finite cross-section and excited by a harmonic point force with a simply supported rectangular model backed with a honeycomb structure is used for separating the cavity into cells.

Results show that each of the honeycomb cells can create local one-dimensional sound fields.

Another application, investigated by Sakagami *et al.*, is thick micro-perforated absorbers for use as interior room finish by themselves only [39]. Use of tapered-hole micro-perforated absorber with varying diameter holes is suggested to obtain good absorption performance.

Mide proposed a configuration with two different sizes of holes on different sides on the same panel of the micro-perforated absorber which are separated by a mid panel perpendicular to the micro perforated panel at the backing air cavity that divides the absorber from the middle [40]. The mid panel also supports the micro-perforated layer. This configuration improves the absorption characteristics of the micro-perforated absorber by enhancing the bandwidth where it is effective. Measurements show that combined benefit of each micro-perforated absorber is observed with a slight decrease of each peak resulted from two hole configurations separately. However, this effect is compensated by the increase at the transition area between the two peaks, thus increasing the effective bandwidth of the absorber. Furthermore, it is also proved that using (micro) perforated mid panel increases the coupling effect between cavities behind the micro-perforated absorber, which further enhances the sound absorption characteristics.

Another application of micro-perforated absorbers is their usage in a passive-active hybrid absorber system, presented by Cobo and Cuesta [41]. Free-field absorption coefficient measurements are made with a large sample, whose configuration is composed of a stationary micro-perforated panel system and a multi-channel active system controlled wooden panel. Perforated panel system composed of a very thin micro-perforated sheet supported with a thick macro perforated panel to overcome the effect of poor absorption characteristics of unsupported thin perforated sheets. Both active and passive measurements are performed and it is seen that with active system, very high increase in absorption coefficients are obtained at low frequencies. Above 500 Hz results are comparable. Pfretzschner *et al.* also worked on the similar perforated system with a micro-perforated sheet backed by a macro perforated sheet

in detail. Results from analytical model, impedance tube measurements and reverberation chamber measurements are compared [42]. The system is named as micro-perforated insertion unit (MIU). Experimental results show good agreement with theory.

For easy design of micro-perforated absorbers, Zhang and Gu worked on a simplified analytic formulae derived from previous studies to predict resonance and anti resonance frequencies of a double layer micro-perforated absorber [43]. Application of a designed absorber in a fan noise problem showed good results.

Fenech *et al.* studied the use of micro-perforated plates to attenuate cavity resonances by introducing damping by acoustic resistance of micro-perforated plate [44]. The model was validated experimentally by comparing predicted Green's functions through measurements of absorption coefficients of a micro-perforated plate mounted in a flat box. The flow impedance of the plate is also determined experimentally.

## **2.5 Sound Transmission and Radiation**

Micro-perforated sound absorbers are not necessarily backed by rigid walls or any other type of rigid backings. In the case of existence of a flexible backing in such absorbers, sound transmission through those non-rigid backings becomes important. Sound transmission through plates with absorptive facings is examined by Takashi [45-47]. Starting from Helmholtz integral equation for two-dimensional problems and providing continuity conditions on surfaces, a procedure for determining transmission loss through single plates with absorptive facings are examined. The first model proposed by Takahashi [45], had some defects: in the model wave motion is assumed as being only normal to surface and anisotropy in absorptive facings is neglected. Takahashi later improved this model to compensate for these defects [46]. Results are validated using an experimental setup, in which transmission loss is measured using reverberation room method. Another improvement on transmission loss of the micro-perforated panel with air cavity and freely vibrating back panel is obtained by insertion of a honeycomb layer to air cavity, which is glued to both

plates [47]. With inserted honeycomb layer, local one dimensional sound field are formed in each of the subdivided cells local and this leads to normal incidence into the orifices. It is also observed that the same motion of the micro-perforated absorber and the back wall would cancel the undesirable effect of the vibration.

Further study on the same topic is performed by Toyoda and Takahashi [48]. They worked on the control of sound radiation from an absorptive plate by using a perforated absorber system, from the viewpoint of acoustic power. Analytic calculations are carried out using mainly Maa's analogy [2] and results show that acoustic radiation depends on change in impedance. Also, it is found that radiation from a vibrating plate can be reduced using an appropriate impedance surface placed at a desired distance from the vibrating plate.

Sound radiation from micro-perforated absorbers may also be a case where absorber is attached to a vibrating surface. Abrahams investigated this phenomenon with a perforated elastic sandwich panel excited by a line force [49]. The radiated far field and unattenuated subsonic plate wave coefficients are found both for air and water as the two media. By the model two distinct unattenuated surface waves, resonances of air gap and plate are examined. Results are not validated by experiments.

It has been demonstrated that micro-perforated absorbers are used in various fields utilizing different materials. It is clear that, there will be various different applications of micro-perforated absorbers in the near future. In this work, development of a micro-perforated absorber from a special type of material is investigated.

## CHAPTER 3

### THEORETICAL DEVELOPMENT

#### 3.1 Introduction

This chapter is dedicated to the development of the mathematical formulation and interpretation of physics associated with the phenomenon. The concept of acoustic impedance will firstly be defined as a basis. With this concept, expressions needed to calculate the resulting acoustic impedance at the very top of an absorber assembly will be listed for prediction of normal incidence absorption coefficients of any micro-perforated absorber. Formulation for characteristic impedance and propagation constant of any layer including a micro-perforated face or plate, porous or fibrous materials or an air cavity that are needed to calculate the impedance at the top of the absorber assembly will be given afterwards. The procedure for calculation of normal incidence absorption coefficient using the calculated impedance at the top of any absorber assembly will be completed at the end of the chapter by introducing the required expressions.

#### 3.2 Acoustic Impedance

Acoustic impedance is an important acoustic parameter, which is a function of frequency. Acoustic impedance is defined as the ratio of acoustic pressure to flow velocity over a defined surface. Analytically, it is the ratio of sound pressure ( $p$ ) divided by the flow (particle) velocity ( $v$ ) and the surface area ( $S$ ) of the propagation medium. Rather than acoustic impedance, specific acoustic impedance is more frequently used in the prediction procedures for absorption coefficients.

Specific acoustic impedance is basically the acoustic impedance divided by the surface area. In general, there is usually a phase relationship exists between pressure and particle velocity depending on the nature of wave propagation. Both acoustic impedance and specific acoustic impedance can be written as a complex value:

$$Z = X + jM \quad (3.1)$$

where  $X$  is the acoustic resistance and  $M$  is the acoustic reactance. Resistance represents loss by various mechanisms, mainly by thermal dissipation, acoustic radiation and reactance represents the ability of medium or layer to store energy of the incident acoustic wave. In the foregoing chapters specific acoustic impedance will be simply noted as impedance ( $Z$ ). The transfer matrix method will be used to deal with multi layer acoustic systems with different media and materials included.

### 3.3 Transfer Matrix Method

Transfer matrix method, is commonly used in acoustics to obtain absorption characteristics of multi layer acoustic absorber systems. In our case, transfer matrix method is used to evaluate impedance and absorption characteristics of any multi layer micro-perforated absorber.

Transfer matrix utilizes surface impedances and impedance of layers using characteristic impedance  $Z_l$  of the layer and propagation constant  $\gamma$ .

The derivation starts with general solution to plane wave equation. General solution for a plane wave traveling in air is simply given as;

$$p = A \exp\left\{j\omega\left(t - \frac{x}{c_0}\right) - \kappa x\right\} \quad (3.2)$$

where  $A$  is a complex constant,  $\omega$  is the angular frequency,  $c_0$  is the speed of sound in air and  $\kappa$  is the attenuation constant.

Assuming a pressure of  $p(0)$  at  $x = 0$  as:

$$p(0) = A \exp \{j\omega t\} \quad (3.3)$$

At  $x = 0$ , pressure of the plane wave as a function of  $x$  can be found using Equations 3.2 and 3.3 as:

$$p = p(0)\exp\{\gamma x\} \quad (3.4)$$

A similar expression for flow velocity can be derived like pressure expression:

$$v = v(0)\exp\{\gamma x\} \quad (3.5)$$

where propagation constant  $\gamma$  is defined as complex sum of attenuation constant  $\kappa$  and phase constant  $\beta$ :  $\gamma = \kappa + j\beta$  and  $\beta = \frac{\omega}{c_0}$

For the derivation of the transfer matrix formula, assume a layer  $l$  with a characteristic impedance  $Z_l$ . The surface impedance at the bottom of the layer is given by  $Z_1$  at  $x=0$  as a result of previous layer, surface impedance  $Z_2$  at  $x=l$  resulting from  $Z_1$  and  $Z_l$ , incident plane wave  $P_i$  and plane wave reflected from the boundary at  $x=0$   $P_r$ . The problem is illustrated in Figure 2.

Impedance (specific acoustic impedance) as a function of  $x$  is defined as:

$$Z(x) = \frac{p(x)}{v(x)} \quad (3.6)$$

In the layer  $l$ , pressure at any point  $x$  can be obtained by superposition of the pressures resulting from the incident and the reflected waves as:

$$p(x) = P_i \exp(\gamma(l-x)) + P_r \exp(-\gamma(l-x)) \quad (3.7)$$

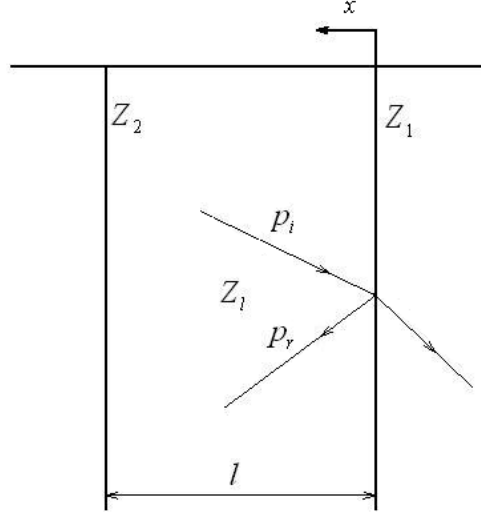


Figure 2. Incident and reflected wave at the boundary  $x=0$

Similarly particle velocity at any point  $x$  by vectoral sum of particle velocities of incident and reflected waves can be obtained as;

$$v(x) = \frac{P_i}{Z_1} \exp(\gamma(l-x)) - \frac{P_r}{Z_1} \exp(-\gamma(l-x)) \quad (3.8)$$

At the boundary interface  $x=l$ , inside the layer  $l$ , surface impedance  $Z_2$  can be found as;

$$\frac{p(l)}{Z(l)} = Z_2 \quad (3.9)$$

Also, total pressure and particle velocity of incident and reflected wave at  $x=l$  is;

$$p(l) = P_i + P_r \quad (3.10)$$

$$v(l) = \frac{P_i}{Z_l} - \frac{P_r}{Z_l} \quad (3.11)$$

Using Equations 3.9, 3.10 and 3.11, magnitude of the reflected wave can be found as:

$$P_r = P_i \frac{Z_2 - Z_l}{Z_2 + Z_l} \quad (3.12)$$

Putting Equations 3.12 into Equations 3.7 and 3.8; expressions for pressure and velocity at  $x = 0$  can be obtained as follows:

$$p(0) = P_i \exp(\gamma l) + P_i \frac{Z_2 - Z_l}{Z_2 + Z_l} \exp(-\gamma l) \quad (3.13)$$

$$v(0) = \frac{P_i}{Z_l} \exp(\gamma l) + \frac{P_i}{Z_l} \frac{Z_2 - Z_l}{Z_2 + Z_l} \exp(-\gamma l) \quad (3.14)$$

At the boundary interface  $x = 0$ , inside the layer  $l$ , surface impedance  $Z_1$  can also be defined as:

$$\frac{p(0)}{v(0)} = Z_1 \quad (3.15)$$

Inserting Equations 3.13 and 3.14 into Equation 3.15 and rearranging terms, the expression for resulting surface impedance  $Z_1$  at  $x = l$  can be obtained as a function of surface impedance  $Z_2$  at  $x = 0$ , impedance of layer  $Z_l$  and propagation constant  $\gamma$  as:

$$Z_1 = Z_l \frac{Z_2 \cosh(\gamma l) + Z_l \sinh(\gamma l)}{Z_2 \sinh(\gamma l) + Z_l \cosh(\gamma l)} \quad (3.16)$$

As a specific case, when any layer is backed by a rigid wall, the impedance  $Z_2$  is thought to be infinite.

When  $Z_2 \rightarrow \infty$ , impedance at the top of the layer can be evaluated as:

$$Z_1 = Z_l \coth(\gamma l) \quad (3.17)$$

Normal incidence absorption coefficients are very useful for determination of absorption characteristics of absorbers. However, they do not supply information on the performance of absorber in random incidence. Random incidence absorption coefficients of an absorber should be known for in situ performance and for acoustic simulation software which include geometric room models. For prediction of random incidence absorption coefficients, two main approaches are available. One of the methods employs wave scattering theory and is out of scope of this work. The other method is proposed by Zou *et al.* [6], which is called as impedance transfer method. In the impedance transfer method a  $\cos\theta$  term with  $\theta$  being the angle of incidence, is multiplied by the propagation constants and impedance values. By introduction of these terms to common formulation, an absorption coefficient as a function of angle of incidence  $\theta$  can be found. By integrating this absorption coefficient over the entire incidence span, an angle averaged value for random incidence absorption coefficient can be obtained.

### 3.4 Impedance of Micro-perforated Layer

Flow in narrow tubes is a special case of fluid motion where viscous loss effects become very important. When the diameter of the tubes (or the holes) is comparable with the thickness of the boundary layer developed, energy dissipation caused by viscous effects becomes significant. Equation for fluid motion in narrow tubes is firstly derived by Lord Rayleigh, and Crandall modified the theory for short tubes [5].

Simplest form of the Navier-Stokes Equation is;

$$\rho \left[ (\vec{v} \cdot \vec{\nabla}) \vec{v} \right] + \frac{\partial \vec{v}}{\partial t} = -\nabla \bar{p} + \rho \vec{g} + \nabla \cdot \mathbf{T} + \mu \nabla^2 \vec{v} \quad (3.18)$$

Where  $(\vec{v} \cdot \vec{\nabla}) \vec{v}$  term represents convective acceleration,  $\frac{\partial \vec{v}}{\partial t}$  is the acceleration related with particle velocity,  $\nabla \bar{p}$  is the pressure gradient,  $\rho \vec{g}$  is the effect of gravitational forces,  $\nabla \cdot \mathbf{T}$  represents stress tensor and  $\mu \nabla^2 \vec{v}$  term is related with viscous forces.

Assuming zero convective acceleration in narrow tube, no effect of gravity in flow and zero stress tensor, the Navier-Stokes equation reduces to:

$$-\nabla \bar{p} + \mu \nabla^2 \vec{v} = \rho \frac{\partial \vec{v}}{\partial t} \quad (3.19)$$

Pressure gradient in cylindrical coordinates is simply:

$$\nabla \bar{p} = \frac{\partial p}{\partial r} + \frac{1}{r} \frac{\partial p}{\partial t} + \frac{\partial p}{\partial x} \quad (3.20)$$

Neglecting radial pressure fluctuations due to narrow tube assumption and steady state pressure with time derivative being equal to zero, pressure gradient reduces to:

$$\nabla \bar{p} = \frac{\partial p}{\partial x} \quad (3.21)$$

Laplacian of the particle velocity in cylindrical coordinate system by assuming particle motion only in  $x$  direction is:

$$\nabla^2 \vec{v} = \nabla^2 v_x = \frac{1}{r} \frac{\partial}{\partial r} \left( r \frac{\partial v_x}{\partial r} \right) + \frac{\partial^2 v_x}{\partial x^2} \quad (3.22)$$

With the assumption of very small fluctuations, second derivative of the particle velocity can be counted as zero hence Equation 3.18 reduces to:

$$\rho \frac{\partial v}{\partial t} = -\frac{\partial p}{\partial x} + \mu \frac{1}{r} \frac{\partial}{\partial r} \left( r \frac{\partial v}{\partial r} \right) \quad (3.23)$$

Assume a plane wave solution for particle velocity in the following form:

$$v = v_0 \exp(j\omega t) \quad (3.24)$$

Time derivative of particle velocity obtained by differentiating Equation 3.24 with respect to time can be rewritten as;

$$\frac{\partial v}{\partial t} = j\omega v \quad (3.25)$$

Hence, Equation 3.23 can be written as:

$$\rho \frac{\partial p}{\partial x} = j\rho\omega v + \mu \frac{1}{r} \frac{\partial}{\partial r} \left( r \frac{\partial v}{\partial r} \right) \quad (3.26)$$

Rearranging terms and defining  $s^2$  as:

$$s^2 = -\frac{j\omega\rho}{\mu} \quad (3.27)$$

The Equation 3.26 reduces to

$$\frac{1}{\mu} \frac{\partial p}{\partial x} = \frac{\partial^2 v}{\partial r^2} + \frac{1}{r} \frac{\partial v}{\partial r} + s^2 v \quad (3.28)$$

The equation above is a non-homogenous Bessel's Equation of order zero. The solution of the differential equation can be obtained as:

$$v = \frac{1}{\mu s^2} \frac{\partial p}{\partial x} + A J_0(sr) \quad (3.29)$$

with  $J_0$  being Bessel's function of the first kind and order zero.

For determination of constant  $A$ , boundary conditions for the narrow tube fluid motion should be defined. The particle velocity at the boundary of the tube should equal to zero. At  $r = R_h$ :  $v(R_h) = 0$ .

Applying this condition to Equation 3.29 results in:

$$\frac{1}{\mu s^2} \frac{\partial p}{\partial x} + A J_0(sR_h) = 0 \quad (3.30)$$

Solving  $A$ , from the Equation 3.30 above and putting in it to Equation 3.29:

$$v = -\frac{1}{j\omega\rho} \frac{\partial p}{\partial x} \left\{ 1 - \frac{J_0(sr)}{J_0(sR_h)} \right\} \quad (3.31)$$

Average particle velocity should be found in order to define the impedance of the micro-perforated layer. Average velocity can be obtained by averaging both sides of Equation 3.31 as:

$$\bar{v} = -\frac{1}{j\omega\rho} \frac{\partial p}{\partial x} \left\{ 1 - \frac{\overline{J_0(sr)}}{J_0(sR_h)} \right\} \quad (3.32)$$

For evaluating average velocity, an average value for the Bessel's function of the first kind of order zero should be found. The average value can simply be written as:

$$\overline{J_0(sr)} = \frac{1}{\pi R_h^2} \int_0^{R_h} J_0(sr) 2\pi r dr \quad (3.33)$$

For evaluating this integral, an integral property of Bessel's function can be used which is:

$$\int_a^b xJ_0(x)dx = bJ_1(b) - aJ_1(a) \quad (3.34)$$

With  $a=0$  and  $b=R_h$ , average value for the Bessel's function can be evaluated using Equation 3.34 as:

$$\overline{J_0(sr)} = \frac{2}{sR_h} J_1(sr) \quad (3.35)$$

Using this average value, average particle velocity can be written using Equation 3.32 as:

$$\bar{v} = \frac{1}{j\omega\rho} \frac{\partial p}{\partial x} \left[ 1 - \frac{2}{sR_h} \frac{J_1(sR_h)}{J_0(sR_h)} \right] \quad (3.36)$$

Assuming a short tube (length of tube is much shorter than the wavelength of the incident sound wave)  $\frac{\partial p}{\partial x}$  value can be approximated as the ratio of pressure difference between entrance and exit of tube to the length of the tube or hole (also length of the plate to which it is drilled)  $t$ :

$$\frac{\partial p}{\partial x} \cong \frac{\Delta p}{t} \quad (3.37)$$

For the ease of representation, a value "h" can be defined as:

$$h = R_h \sqrt{\frac{\omega\rho_0}{\mu}} \quad (3.38)$$

By defining h,  $sR_h$  can be written as:

$$sR_h = h\sqrt{-j} \quad (3.39)$$

Specific acoustic impedance for a single hole can be defined using the definitions above as:

$$\frac{\Delta p}{v} = Z_{hole} = j\omega\rho_0 t \left[ 1 - \frac{2}{h\sqrt{-j}} \frac{J_1(h\sqrt{-j})}{J_0(h\sqrt{-j})} \right] \quad (3.40)$$

Impedance of a hole in the perforated layer is not simply composed of the impedance of a single hole. According to Cox and D'Antonio [50], additional terms for radiation resistance for an orifice and a term covering the end correction for the radiation reactance of the tube should be added to expression of impedance. Acoustic impedance for the perforated layer with terms for radiation resistance and end correction added can simply be written as:

$$Z_{hole,m} = Z_{hole} + \frac{\sqrt{2\omega\rho\mu}}{2} + j1.7\omega\rho R_h \quad (3.41)$$

Using the corrected expression for impedance of a hole, impedance of the perforated layer can be calculated by dividing the impedance values by the perforation constant  $\varepsilon$ , which is defined as the ratio of surface area of the perforations to the total surface area of the layer.

$$Z_{perf} = \frac{Z_{hole,m}}{\varepsilon} + \frac{\sqrt{2\omega\rho\mu}}{2\varepsilon} + \frac{j1.7\omega\rho R_h}{\varepsilon} \quad (3.42)$$

$$\varepsilon = \frac{\pi R_h^2}{a^2} \quad (3.43)$$

Total acoustic impedance at the top of a perforated layer is simply the sum of acoustic impedance at the top of any previous layer (or at the bottom of the micro-perforated layer) and acoustic impedance of micro-perforated layer (apart from transfer matrix equation, Equation 3.16) as

$$Z_{top} = Z_{total} + Z_{perf} \quad (3.44)$$

### 3.5 Impedance of Porous Layer

Dissipation of acoustic energy while waves are traveling in porous absorbers takes place by friction like dissipation in perforations. Closely placed, dense, thin fibers make up a medium with very small air gaps between fibers and acoustical energy is transformed into heat with boundary layer friction and vibration of fibers, which is also damped by the contact between fibers.

Even if, the best way to obtain characteristics of a porous absorber is to directly measure characteristic impedance and propagation constant of the material, this is not that easy and it is not feasible in most cases. Various empirical models were developed for determining propagation of sound waves in porous absorbers. Existing empirical models are mainly obtained through various controlled measurements using different samples and different types of porous materials. This kind of general approach covering all kinds of porous materials in a single set of equations leads to moderate levels of error [9].

The two main parameters used to define acoustical characteristics of a medium are characteristic impedance  $Z_{po}$  and propagation constant  $\gamma_{po}$ , which are basically functions of the following parameters: flow resistance  $R_f$ , density of air  $\rho$ , speed of sound of air  $c_0$ , frequency  $f$  (or angular frequency  $\omega$ ).

Even there are various models in literature for determination of these two parameters, in this work, the model proposed by Delany and Bazley [9] is used. In this model, expressions for characteristic impedance and propagation constant are given as:

$$Z_{po} = \rho c_0 \left[ 1 + 0.0571 \left( \frac{\rho f}{R_f} \right)^{-0.754} - j0.087 \left( \frac{\rho f}{R_f} \right)^{-0.732} \right] \quad (3.45)$$

$$\gamma_{po} = \frac{j\omega}{c_0} \left[ 1 + 0.0978 \left( \frac{\rho f}{R_f} \right)^{-0.700} - j0.189 \left( \frac{\rho f}{R_f} \right)^{-0.595} \right] \quad (3.46)$$

If any porous layer is backed by a rigid wall, acoustic impedance at the top of the porous layer  $Z_{porous}$  can be evaluated as [8]:

$$Z_{porous} = -jZ_{po} \coth(\gamma_{po} t_{po}) \quad (3.47)$$

with  $t_{po}$  being the thickness of the porous layer.

### 3.6 Impedance of Air Cavity

Similarly, characteristic impedance and propagation constant of air can be found as [8],

$$Z_a = \rho_0 c_0 \quad (3.48)$$

$$\gamma_a = jk_a \quad (3.49)$$

with  $k_a$  being wave number of air.

If air cavity is backed by a rigid wall, acoustic impedance at the top of the cavity can be evaluated as [8],

$$Z_a = -j\rho_0 c_0 \coth(k_a t_a) \quad (3.50)$$

with  $t_a$  being depth of the cavity.

### 3.7 Determination of Absorption Coefficient

The characteristic impedances and propagation constants of the micro-perforated plate, the porous absorber and air cavity is defined layer by layer in order to be used in transfer matrix method to obtain absorption coefficient in the previous sub-chapters. Also, any absorbent layer with specified characteristic impedance and specified propagation constant can be used in transfer matrix method for obtaining the total acoustic impedance of a given absorber configuration. Having the transfer matrix equation 3.16, with acoustic impedance at the surface of the very top layer being  $Z_{total}$ , the reflection coefficient  $R$  can be calculated as [49]:

$$R = \frac{Z_{total} - \rho_0 c}{Z_{total} + \rho_0 c} \quad (3.51)$$

Using the reflection coefficient  $R$ , normal incidence absorption coefficient  $\alpha$  can be obtained using formula [49]:

$$\alpha = 1 - |R|^2 \quad (3.52)$$

## CHAPTER 4

### ANALYTICAL MODELING

#### 4.1 Overview of Analytical Model

The analytic model is built up with the help of analytic expressions derived in previous chapter. A routine for the analytic model is coded using MATLAB<sup>®</sup>. In the MATLAB<sup>®</sup> code, subroutines for micro-perforated layer, for fibrous layer of Parabeam<sup>®</sup>, and also for any possible air cavity and common fibrous material (glass wool, mineral wool) layers is developed.

With the configuration of any absorber input to MATLAB<sup>®</sup> code, total acoustic impedance at the top of the absorber assembly calculated step by step by each layer with the help of Equation 3.16. Reflection coefficient and normal incidence absorption coefficients are calculated respectively from the acoustic impedance by Equations 3.51 and 3.52. The routine calculates normal absorption coefficients in octave band frequencies and outputs the absorption coefficient vs. frequency graph.

The input to MATLAB<sup>®</sup> code is supplied by typing a matrix with any name (let us denote matrix with name “A”) with four columns and n+1 rows (n: number of layers in the absorber assembly) to the command window of MATLAB<sup>®</sup> containing the required information for all layers of the absorber assembly.

In the input matrix, definition of the layers are made with numbers in the first column, starting from the bottom with: (1) for micro-perforated layer, (2) for air layer, (3) for porous-fibrous absorber layer, (4) for mid layer of Parabeam<sup>®</sup> with

thick fibers, (0) to define the end of absorber. Other elements of the definition matrix for each layer can be defined by the parameters:

- For micro-perforated layers: thickness of the micro-perforated layer, diameter of holes and perforation ratio which are placed in the second, third and fourth columns, respectively.
- For air layers: thickness of the air layer placed in second column and (0) for other columns.
- For porous-fibrous absorber layers: thickness of porous-fibrous absorber, flow resistivity of the absorbing material for second and third columns, respectively and “0” for the fourth column.
- For mid layer of Parabeam<sup>®</sup>: (0) for all second, third and fourth columns. (Since there is no existing mathematical model for this layer, the values needed for calculation procedure is calculated using the finite element model with details explained in the next chapter. The definition of the layer in the first column calls acoustic impedance for each 1/3 octave band center frequency for this layer that are already defined inside the routine.)

With definition of the input data, the m-file for calculation of absorption coefficients of the absorber assembly input is called by typing “*perforated(A)*” to command window of MATLAB<sup>®</sup> (“A” denotes the name of the input matrix).

The code for the analytical model is given in APPENDIX A.

## 4.2 Results

For verification of the models, four samples of different micro-perforation configurations are used. Apart from unchanged parameters: thickness of the fibrous layer  $t_f = 18mm$ , thickness of the micro-perforated layer  $t_p = 1mm$ , the two parameters: the distance between holes in the square grid  $a$  and radius of holes  $r$  are varied. Sample configurations are given in Table 2.

The matrix input to MATLAB<sup>®</sup> is changed for each sample configuration. Results for absorption coefficients in each run of the routine for each sample are illustrated in Figures 3-6. Acoustic impedance values of the fibrous part of Parabeam<sup>®</sup> are obtained from the finite element solution to be discussed in detail at the next chapter.

Table 2: Sample Configurations

Sample #	a (mm)	r (mm)
1	16	0.5
2	8	0.5
3	16	0.25
4	8	0.25

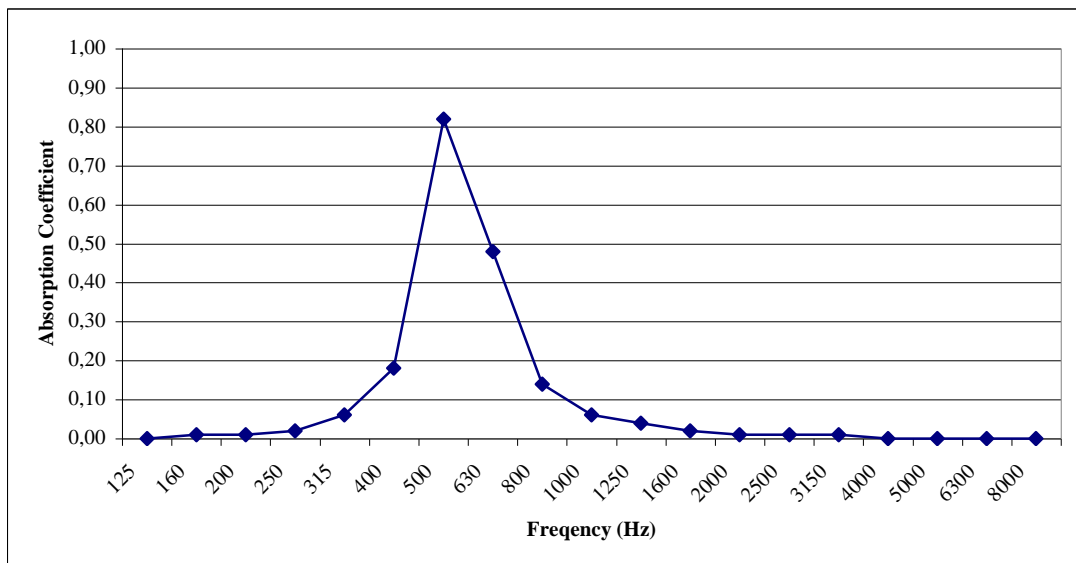


Figure 3. Predicted normal incidence absorption coefficients for Sample 1 obtained from analytical model

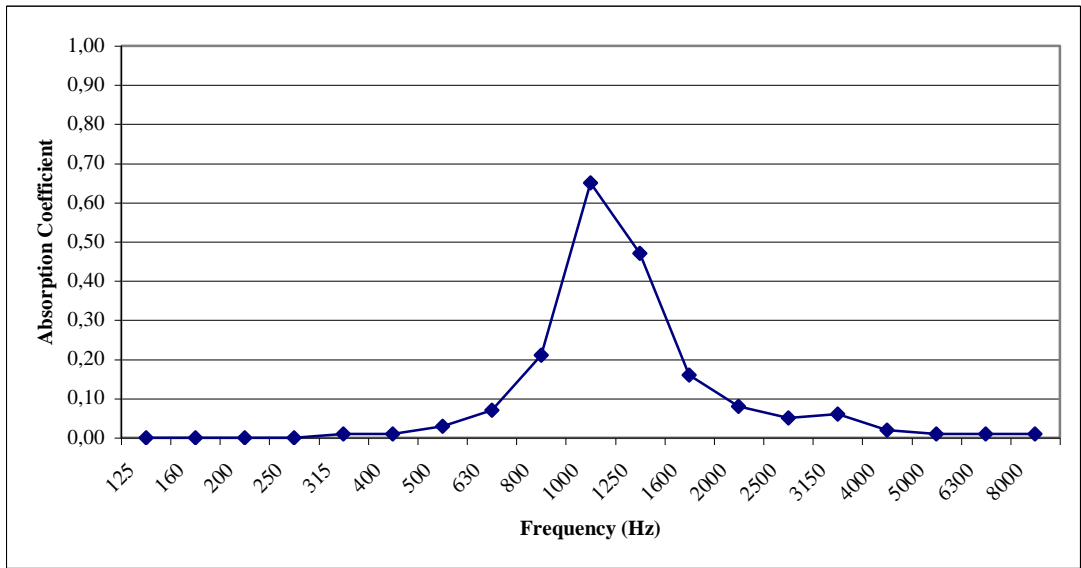


Figure 4. Predicted normal incidence absorption coefficients for Sample 2 obtained from analytical model

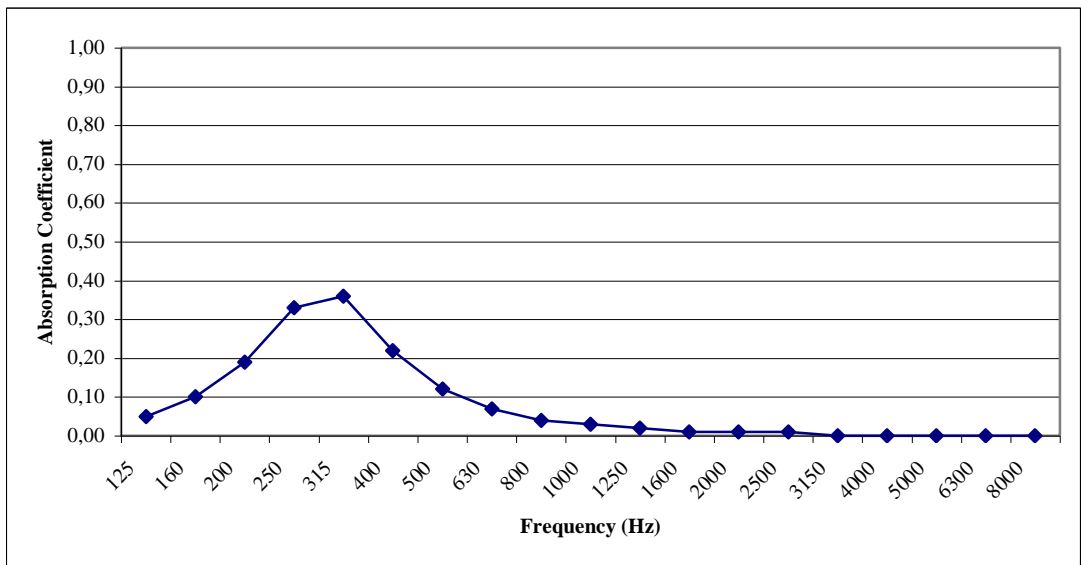


Figure 5. Predicted normal incidence absorption coefficients for Sample 3 obtained from analytical model

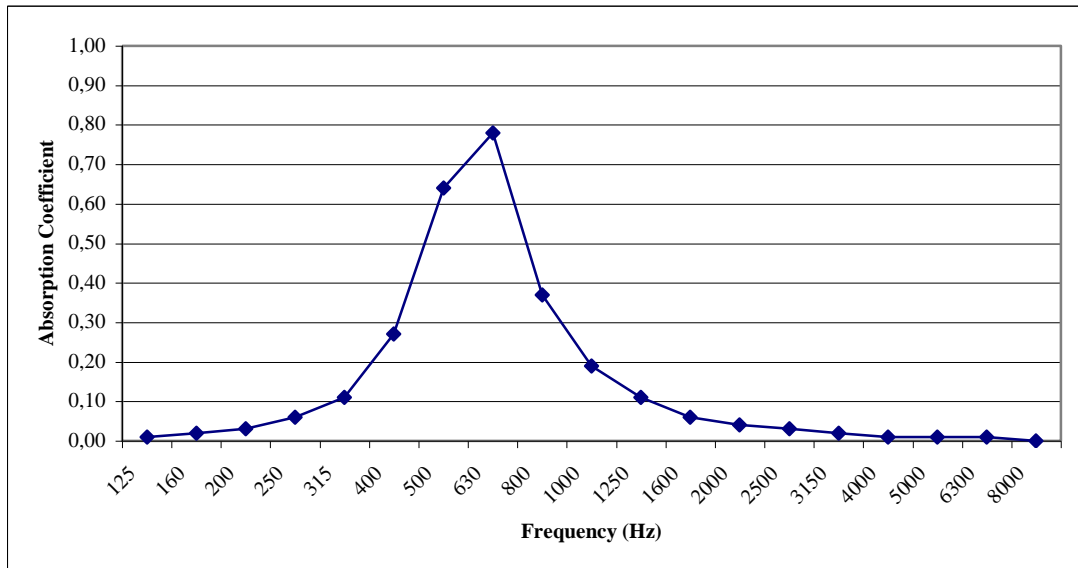


Figure 6. Predicted normal incidence absorption coefficients for Sample 4 obtained from analytical model

The peak values observed in samples 1 and 2 is the result of the micro perforations and the distance between perforated layer and bottom layer. Change in the frequency where the absorption peak observed is caused by the change in perforation ratio  $\varepsilon$  (or by change in hole spacing since hole diameters for sample 1 and 2 is same). Several runs of MATLAB<sup>®</sup> code with different values for hole spacing and hole diameter show that effective absorption can be obtained in a relatively narrow frequency band. Even if, changes in hole spacing results in shift of frequency of the absorption peak, it is seen that effective absorption can be obtained in a frequency band covering 2 or 3 octaves with peaks at 500 Hz and 1000 Hz. Consecutive runs of the analytical model show that it is not possible to obtain peaks with high absorption values at higher or lower frequencies.

## CHAPTER 5

### FINITE ELEMENT MODELING

#### 5.1 Finite Element Modeling

Finite element modeling and solution is another method proposed for prediction of absorption coefficients of acoustic materials. Prediction of the effect of fibers inside Parabeam<sup>®</sup> can only be obtained by the finite element solution. Any analytical or empirical model in literature does not exist for impedance of such a layer which contains thick fibers and very high void ratio. Common models are built up and validated for fibrous absorbers work for prediction of materials with micro diameter fibers and fiber volume to total volume ratios above 95 % [9]. Thus, for prediction of the fibrous layer and also for prediction of absorption coefficient of the whole absorber, a finite element model is built by the commercial software MSC.PATRAN and finite element solution is performed using the commercial acoustic finite element solver, MSC.ACTRAN software [51]. In the existing literature, there are some examples of use of finite element solution for prediction of normal incidence absorption coefficients [28-30]. In these examples, codes are built for the finite element solver. Since, an acoustic finite element solver is already available in MSC.ACTRAN; such approach including writing separate codes is avoided.

In the finite element modeling procedure, a simplified 3D solid model of the absorber and air at the top of the micro-perforated layer is created and meshed in MSC.PATRAN with the acoustic elements of the MSC.ACTRAN material library. Since the exact model of Parabeam<sup>®</sup> is not available, the model includes a small portion of the absorber with a simplified geometry and mainly keeping ratio of total fiber volume to volume of the whole cavity, which is around 15 %. Care has been

exercised to keep the profile and cross section of modeled fibers as close as to the real fibers. A simple illustration of the model can be seen in Figure 7. In the finite element solution a very high modulus of elasticity value is assigned to solid elements with the assumption of rigid and stationary fibers.

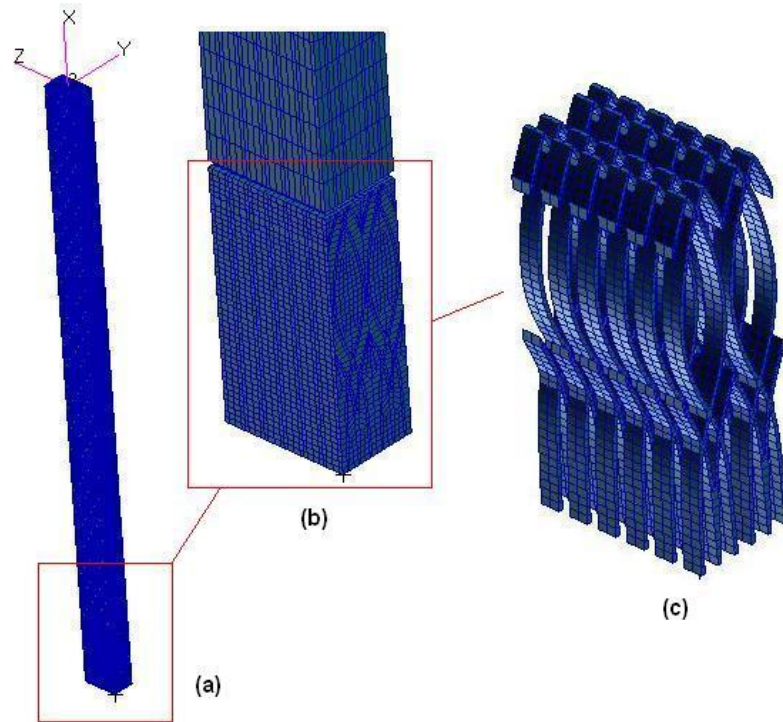


Figure 7. A general view of finite element model with whole model (a), a closer view to absorber (b) and fibers modeled inside the cavity (c)

Air cavity inside the Parabeam and air placed at the top of the perforated layer is meshed with fluid elements and thick fibers are modeled with elastic solid elements [50]. An MSC.ACTRAN boundary layer condition is applied to model the micro-perforated layer rather than directly modeling the micro-perforated layer. The plate and the holes and surrounding air are not meshed separately. This method of modeling by defining such an interface utilizing Mechel's formula for micro perforations is proposed by MSC.ACTRAN [51] and it avoids fine meshing, which is

time consuming both in modeling and solution processes. The interface defined includes two coupling surfaces with one placed at the upper surface of the air elements inside Parabeam<sup>®</sup> and second surface placed at lower surface of air elements at the top of micro-perforated layer physically. Between these two coupling surfaces, the relations of micro perforation are defined by introducing the “transfer admittance” calculated from Mechel’s formula [51] for each frequency, which defines the relation between pressure and velocity between two coupling surfaces. Also, the defined interface for use with different micro perforation configurations evades the necessity of rebuilding of model for each configuration. The four different samples and an optimized case are analyzed by only changing the required lines of interface definition in the analysis input file.

The finite element model is composed of 50592 3D elements of air and fibers. There are 46288 3D fluid elements with properties of air including 200 WEDGE6 and 46088 HEX8 elements and there are 4008 3D elastic solid elements with properties of fiber including 96 WEDGE6 and 3912 HEX8 elements [50]. Also, there exist 1152 2D QUAD elements of interfaces and modal excitation. The absorber model built corresponds to a sample size of 6 x 9.6 mm and thickness of 18 mm. Average edge length of the elements is around 0.5 mm.

Modal Basis property in Analytic Module of the MSC.ACTRAN is used as excitation to the model [50]. In the Model Basis, a modal acoustic excitation in terms of duct modes is introduced to the system. The resulting duct modes are identified in terms of transversal and longitudinal wave numbers and average modal intensities of the incident and reflected waves are computed. With the modal basis input to the data file of the finite element model, MSC.ACTRAN solves for the resulting duct modes of the modal basis.

The acoustic field modeled by finite elements is coupled along a set of free faces to an analytical representation of the sound field in a duct. The sound field in the duct is the combination of a known incident sound field (+) and of an unknown reflected sound field (-). Both the incident and reflected sound fields are defined as linear combinations of duct modes [50].

The faces along which the coupling occurs between the finite elements and the analytical modal component are defined in the MODAL SURFACE data block of MSC.ACTRAN [50]. The theory of modal solution is given in Appendix B. The analytical modal component is defined in the MODAL BASIS data block, which contains the information of cross-section geometry and half-width values of the cross section. A local coordinate system is also defined with the first axis being coincident with the duct axis and the second and the third local axis defining the transverse plane. An acoustic material with air property is assigned to the elements of the modal basis.

In the modal basis, the acoustic field in the duct can be defined by any number of modes. In MSC.ACTRAN, each mode is characterized by its three orders  $(l,n,m)$ . In the finite element model developed, two modes are used:  $(+1,0,0)$  and  $(-1,0,0)$ . The first order ( $l$ ) defines the propagation direction, in which “+1” means along the positive direction of the duct axis of the duct and “-1” means in the opposite direction, the second and third order  $(n,m)$  are respectively the order along the axes other than the axis of propagation. These axes are the ones previously defined by a local coordinate system. Also, the first mode is constrained as the excitation mode as “AMPLITUDE {1,0}” in data block and second mode is constrained without any conditions and is defined as “FREE”.

With the modal basis input to the data file of the finite element, MSC.ACTRAN solves for the resulting duct modes of the modal basis. In the results file, duct mode 1002 represents the average intensity of the reflected wave in the prescribed frequencies. By multiplying the average intensity values with the cross section area of the duct, reflection coefficient can be obtained and using the reflection coefficient the absorption coefficient for the absorber can be calculated through Equation 3.52.

## 5.2 Determination of the Acoustic Impedance at the top of the Fibrous Layer of Parabeam<sup>®</sup>

A model, very similar to the model built for prediction of absorption coefficients is developed for prediction of acoustic impedance at the top of the fibrous layer of Parabeam<sup>®</sup>.

The model prepared for acoustic impedance prediction has some minor differences from the model for absorption coefficient prediction. One difference is the gap between the top of fibrous layer of Parabeam<sup>®</sup> and the air at the top is filled with 3D fluid elements with air property connecting the two sides. Also, the interface boundary layer condition and related 2D QUAD elements is removed from the model, which simulates the micro-perforated layer.

For determination of the acoustic impedance, several 'Field points' are defined in the input file of the finite element model. An overview of the finite element model built for determination of the acoustic impedance at the top of the fibrous layer is illustrated in Figure 8. The points are defined at the top face nodes of the 3D fluid elements, which are placed at the top of the fibrous layer of Parabeam<sup>®</sup>. At these 'Field points', complex acoustic pressure and complex particle velocity values in x, y and z directions are stored separately, in the output file of the finite element solution. Complex particle velocity can be obtained by multiplying the complex displacement values by  $j\omega$ . Acoustic impedance, at the top of the of the fibrous layer of Parabeam<sup>®</sup> can be evaluated by dividing averaged complex pressure by the averaged particle velocity at the 'Field points', as designated in Equation 3.6.

The finite element model for acoustic impedance prediction is composed of 50976 3D elements including 296 WEDGE6 and 50680 HEX8 elements and fibers and also 384 2D QUAD elements of modal excitation corresponding to a sample absorber size of 6 x 9.6 mm and thickness of 18 mm. Average edge length of the elements is around 0.5 mm. The acoustic impedance is calculated and illustrated in the Figure 9, with real and imaginary parts given separately.

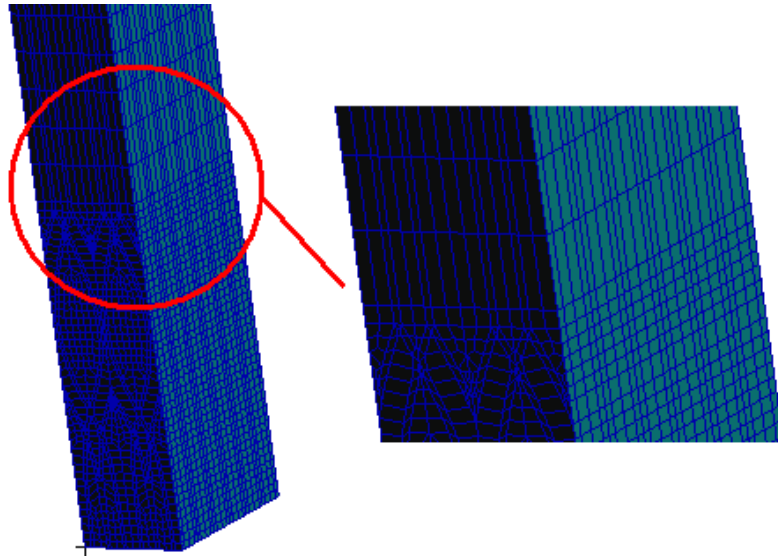


Figure 8. An illustration of model built for determination of acoustic impedance at the top of the fibrous layer with the space between middle and top filled with air elements

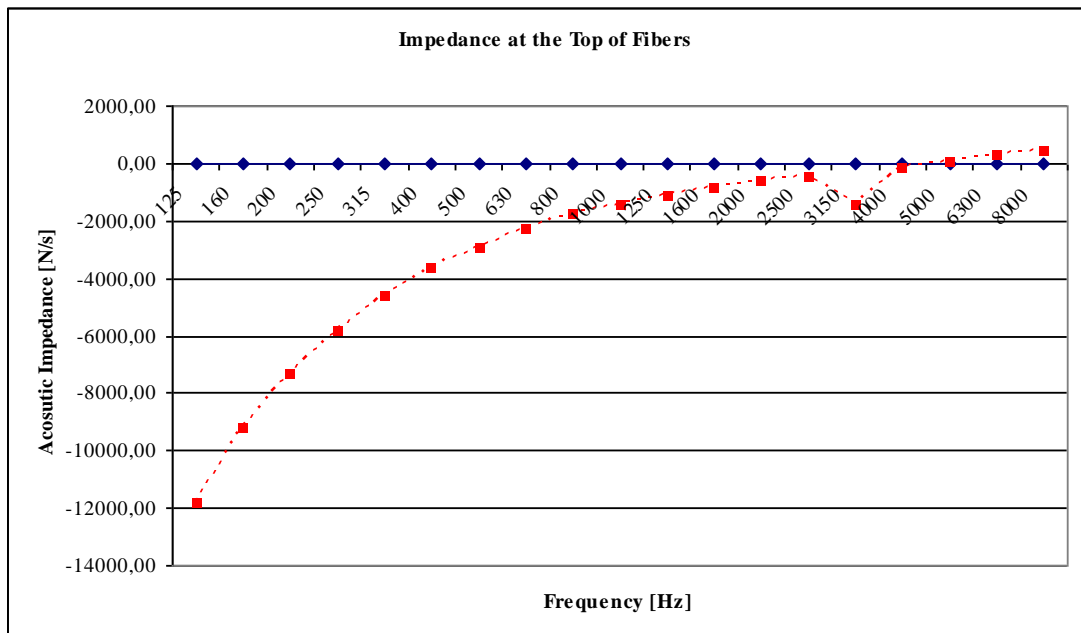


Figure 9. Real and imaginary parts of acoustic impedance at the top of fibrous layer obtained from finite element modeling: real part (blue-solid), imaginary part (red-dotted)

### 5.3 Results of Predictions of Normal Incidence Absorption Coefficients from Finite Element Model

Predictions for normal incidence absorption coefficients are obtained for each sample using the model described in Chapter 5.1. The predicted absorption coefficients are illustrated in Figures 10-13 for each sample.

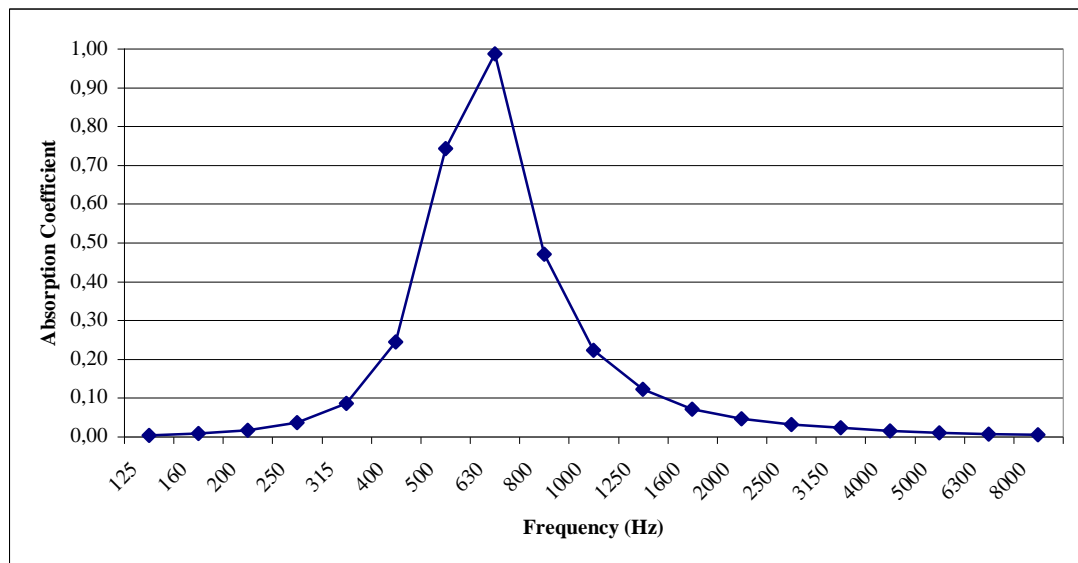


Figure 10. Predicted normal incidence absorption coefficients for Sample 1 obtained from finite element model

The result of finite element model show similar characteristics with results obtained from the analytical model with peaks at 500 Hz and 1000 Hz for samples 1 and 2. Also, some absorption is observed at other frequencies around 500 Hz and 1000 Hz. The general character of the absorption curves is very similar to analytical model predictions except for Sample 3. For Sample 4, finite element predictions are much higher than values obtained from analytical model compared with Sample 1 and 2.

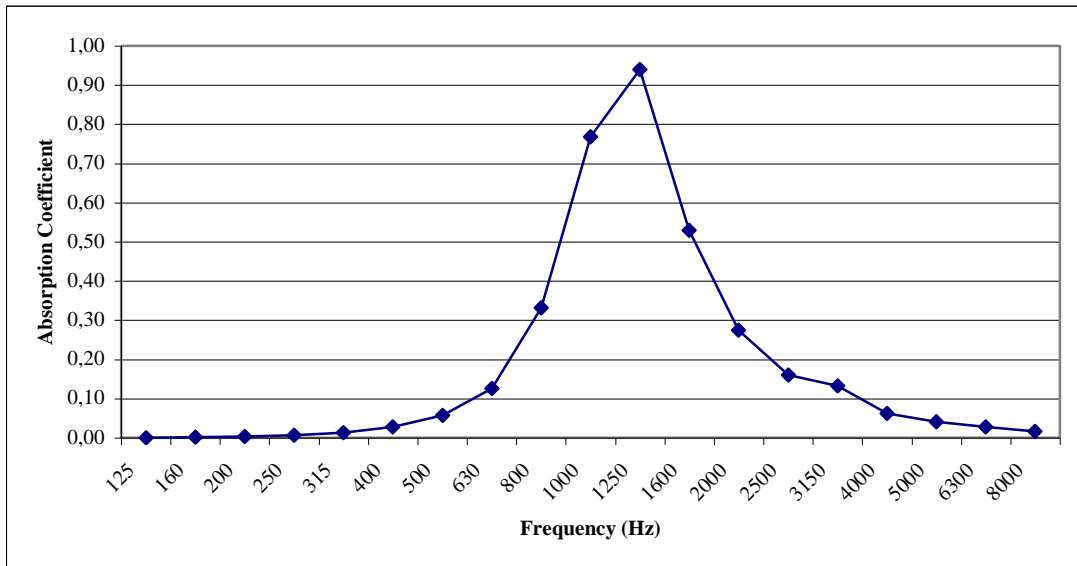


Figure 11. Predicted normal incidence absorption coefficients for Sample 2 obtained from finite element model

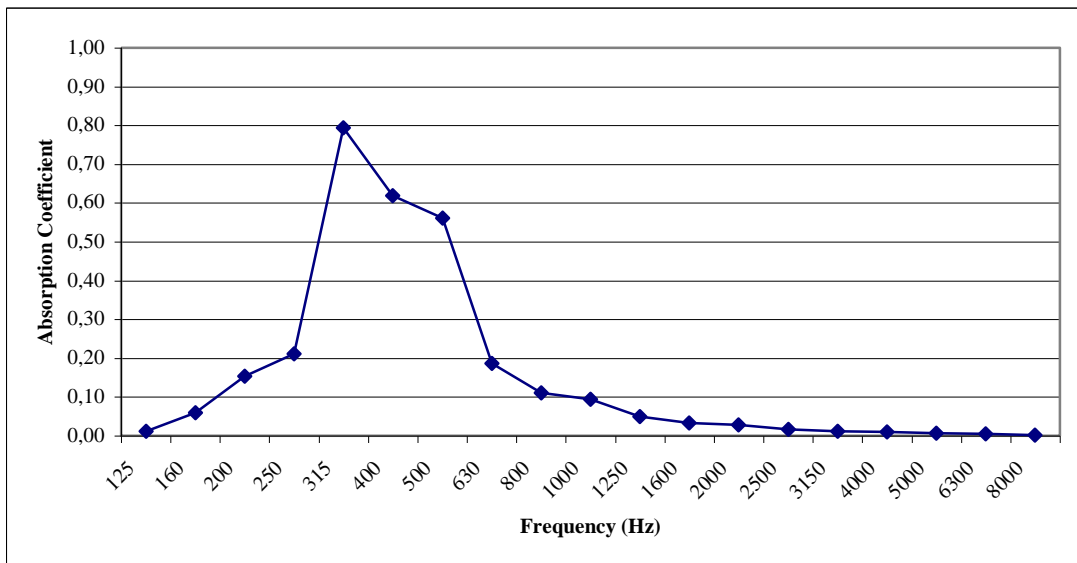


Figure 12. Predicted normal incidence absorption coefficients for Sample 3 obtained from finite element model

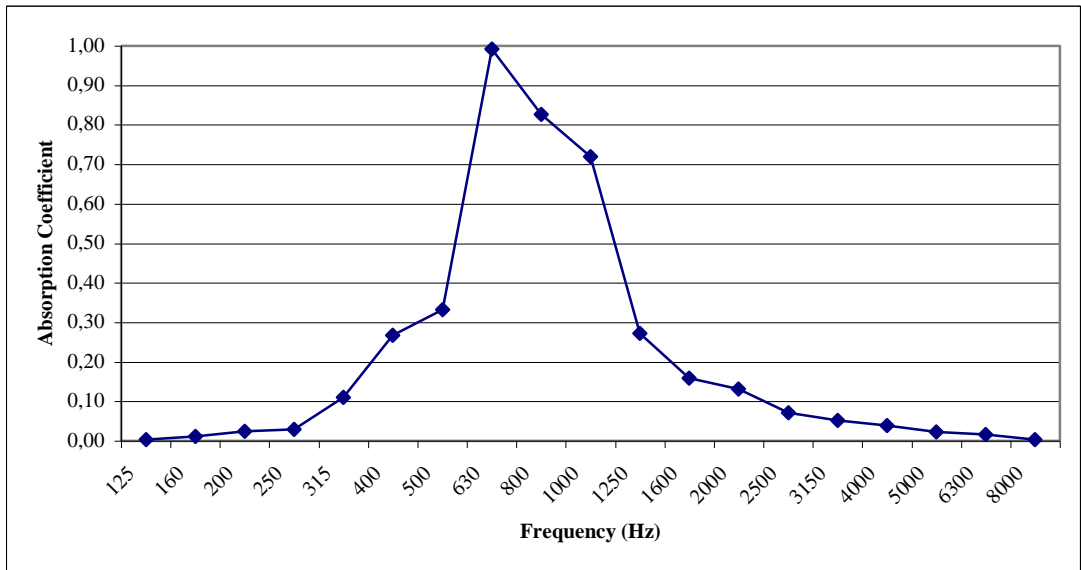


Figure 13. Predicted normal incidence absorption coefficients for Sample 4 obtained from finite element model

## CHAPTER 6

### EXPERIMENTAL RESULTS

#### 6.1 Measurement Set-up

Measurements are performed using a standing wave tube setup with 6.9 cm of tube internal diameter. Normal incidence absorption coefficients of the samples are measured according to standard: ISO 10534-2:1998, “Acoustics - Determination of sound absorption coefficient and impedance in impedance tubes - Part 1: Method using standing wave ratio” [52].

Impedance tube enables both normal incidence absorption coefficient and surface impedance to be measured in a controlled environment. Impedance tube measurements are frequently used in validating prediction models for normal incidence absorption coefficients. The method has the advantage of using very small samples of the materials to be measured compared with the large size samples used in reverberation chambers. Small samples can easily be constructed in large numbers and with different configurations inexpensively compared with large samples used in reverberation chamber measurements. Apart from these, impedance tube measurements can be carried out with relatively simple standard apparatus, without any large chambers or rooms at high costs.

In a typical impedance tube, a loudspeaker placed in one end generates plane waves that are propagating along the axis of the impedance tube. The plane waves propagate down the other end of the tube before being reflected from the sample. A standing wave is set up in the impedance tube by superposition of the reflected and

incident wave [50]. Through measurement of amplitude of the resulting standing wave, it is possible to calculate the normal incidence absorption coefficient and surface impedance of the sample.

There are two main methods for measurement of normal incidence absorption coefficients in impedance tubes, namely, standing wave method and transfer function method. Standing wave method is utilized in this study.

The standing wave method impedance tube setup used in this work involves a transparent plastic tube fitted at one end with a twin loudspeaker enclosure, and at the other hand a heavy sample holder on which the sample material is mounted. A small microphone can be axially moved along the length of the tube. The loudspeakers are fed with a variable common pure tone (single frequency) from a function generator, whose signal is amplified by the amplifier before being fed into the loudspeakers. With the aid of the oscilloscope, the amplitude of maximum and minimum signals received by the traveling microphone is measured. A schematic of the experimental set-up is shown in the Figure 14 below.

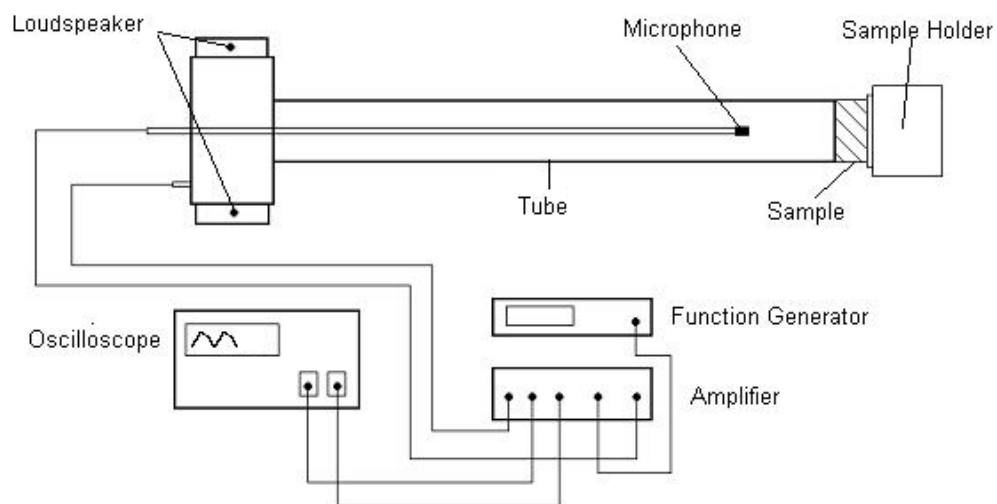


Figure 14. A schematic of the standing wave impedance tube set-up

The measurement procedure involves measurement of root mean square (rms) pressure by measurement of amplitude of signal sensed by microphone (in mV) at the node (maximum pressure) and the antinodes (minimum pressure) of the standing wave at the specified frequency to which the signal is fed through the loudspeaker. The method is very reliable and easy. Unfortunately, measurement of only one frequency at a time is possible. Measurement of the absorption coefficient through a continuous frequency span is not feasible. The procedure of locating positions where maximum and minimum pressure values occur is rather slow and needs much attention [49].

The steady state pressure in the tube can simply be written as a result of both incident and reflected wave as:

$$p = A[e^{jkz} + R.e^{-jkz}] \quad (6.1)$$

where  $R$  is the reflection coefficient,  $k$  is the wave number, with sample is assumed to be located at  $z = 0$  and  $A$  is a complex constant. First term represents the incident wave and second term represents the reflected wave. Maximum pressure  $p_{\max}$  occurs when incident and reflected waves are in phase and minimum pressure  $p_{\min}$  occurs when they are out of phase.

Maximum pressure and minimum pressure in terms of reflection coefficient  $R$  can be written as:

$$p_{\max} = 1 + |R| \quad (6.2)$$

$$p_{\min} = 1 - |R| \quad (6.3)$$

Using these two values, standing wave ratio ( $SWR$ ) can be defined as the ratio of amplitudes of maximum pressure to minimum pressure:

$$SWR = \frac{P_{\max}}{P_{\min}} = \frac{1 + |R|}{1 - |R|} \quad (6.4)$$

The equation above can be rearranged such that leaving  $R$  alone:

$$|R| = \frac{SWR - 1}{SWR + 1} \quad (6.5)$$

The normal incidence absorption coefficient can then be determined using Equation 3.52 as  $\alpha = 1 - |R|^2$ .

Although standing wave impedance tube method has many advantages, there exist some limitations for using this method. Some general limitations are discussed as follows:

- The losses into and through the tube should be minimized. Surface finish inside the tube should be good. If considerable absorption inside the tube is foreseen, effect of tube absorption should be included in Equation 6.1 [49].
- The microphone should be kept at a minimum distance of two times the tube diameter from the loudspeaker and from the sample to avoid cross modes [49].
- Any gap between the sample and the tube should be avoided to be able to eliminate edge effects resulting in false absorption values.
- Upper frequency that can be measured in a tube is determined with the following equation [49]:

$$f_u = \frac{c_0}{2d} \quad (6.6)$$

with  $d$  being the diameter of the tube, which assures no cross modes occurring inside the tube. The diameter of the impedance tube used in measurements is 69 mm. The upper frequency limit for the impedance tube used can then be calculated as 2464 Hz. The predictions illustrated in previous chapters cover a frequency span up to

8000 Hz. Even there exist frequencies, which are out of the range of capability of the impedance tube, the predictions show that there is almost no absorption at these two frequencies so measurements above 2000 Hz will be illustrated as zero.

## 6.2 Results of Impedance Tube Measurements

The measurements are performed in Dynamic Systems Laboratory in Mechanical Engineering Department of Middle East Technical University. The impedance tube measurements are performed on a Hilton B400 Acoustic Insulation Test Apparatus. The set up involves: a clear rigid plastic impedance tube which has 69 mm internal diameter and 1.2 m length, a twin loudspeaker system housed in an enclosure, a dense Tufnol plug sample holder, GW Function Generator of type GFG 8020G, a dual beam 20 MHz Oscilloscope of model GW GOS-622B and Hilton B400 Test Apparatus consisting of signal generator and impedance tube. The experimental setup and the samples used in measurements can be seen in Figure 15 and Figure 16, respectively.

Results of the measurements for each sample are illustrated in Figures 17-20.



Figure 15. The experimental set-up used in impedance tube measurements



Figure 16. The samples used in measurements

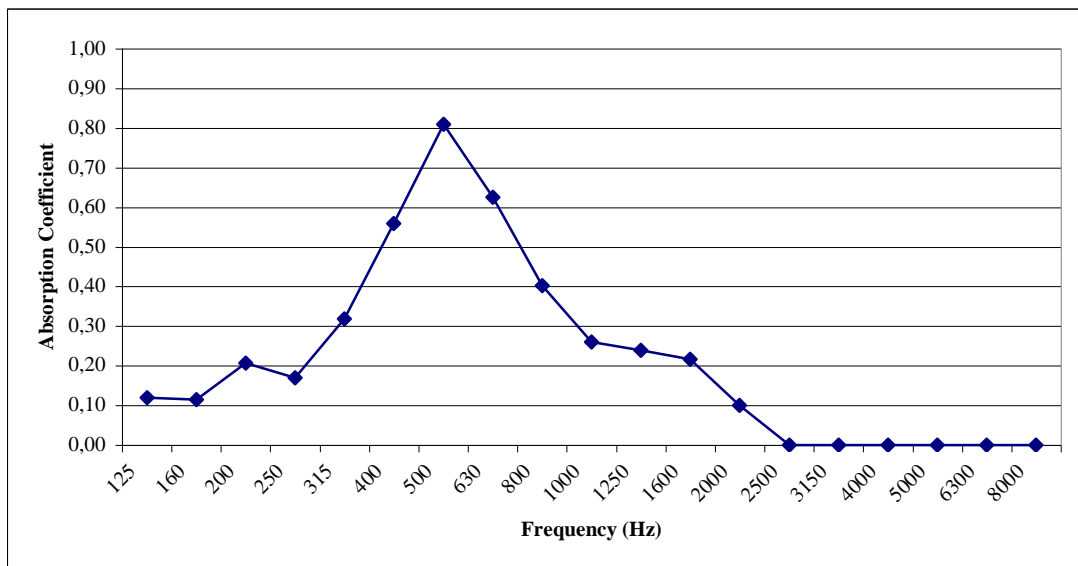


Figure 17. Measured normal incidence absorption coefficients for Sample 1

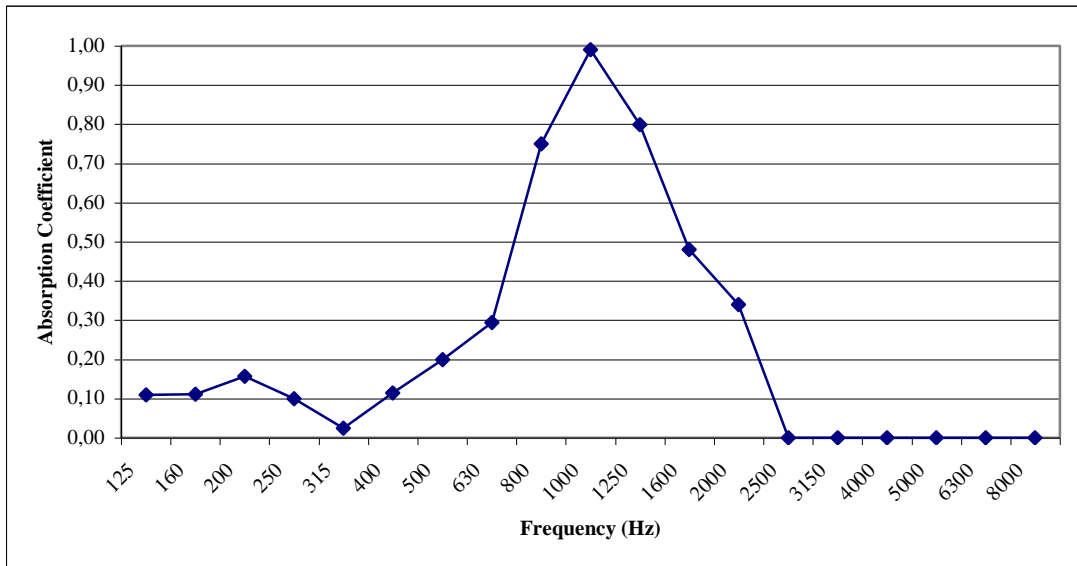


Figure 18. Measured normal incidence absorption coefficients for Sample 2

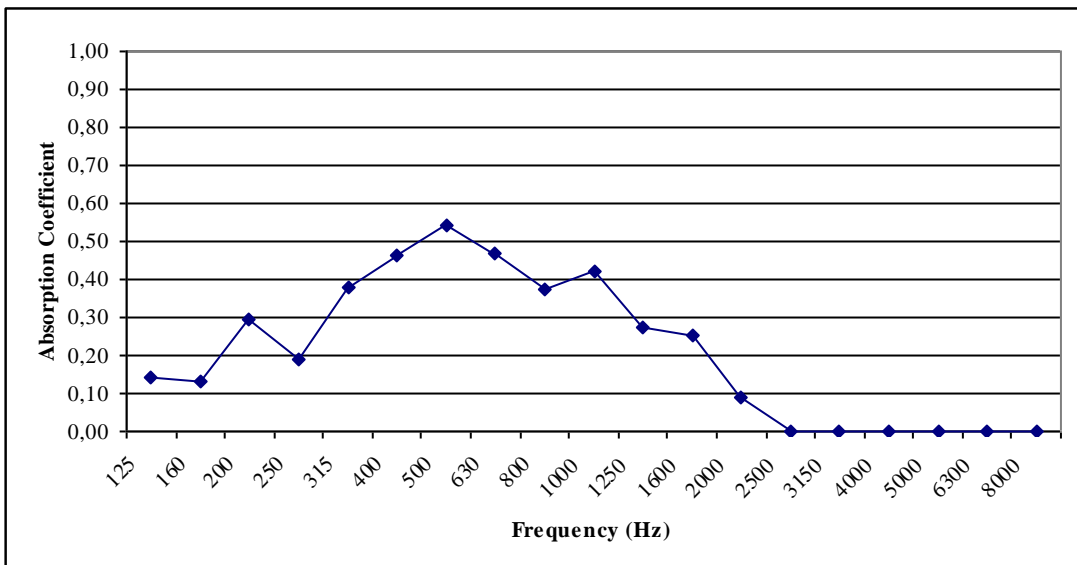


Figure 19. Measured normal incidence absorption coefficients for Sample 3

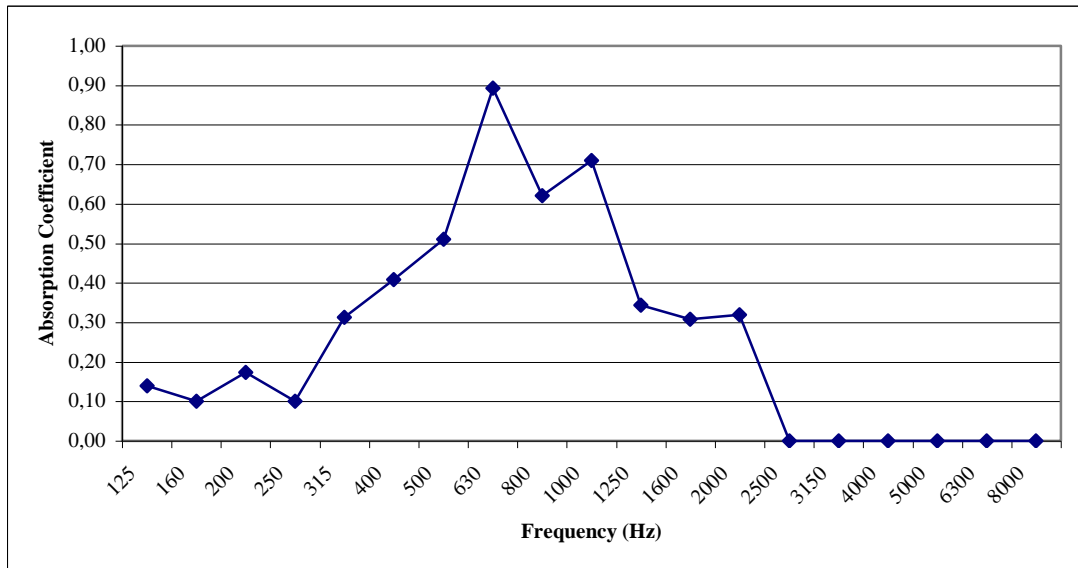


Figure 20. Measured normal incidence absorption coefficients for Sample 4

In the measurements, absorption coefficient for each sample at 1/3 octave band center frequencies are measured using the procedure outlined in this chapter. Similar absorption characteristics like analytical model and finite element results are observed in impedance tube measurements for Samples 1, 2 and 4 with absorption mainly concentrated at 500 Hz and 1000 Hz. For sample 3, there are frequency shifts at peak absorption frequencies both from analytical and finite element model. A detailed comparison of the results from analytical model, finite element model and impedance tube measurements are presented in the next chapter.

## CHAPTER 7

### COMPARISON OF RESULTS AND OPTIMIZATION

#### 7.1 Comparison of Results

In Chapters 4-6, normal incidence absorption coefficients of four samples of the micro-perforated absorber built from Parabeam<sup>®</sup> are predicted using the developed analytical and finite element models and impedance tube measurements are performed in a standing wave impedance tube setup. The predicted absorption coefficients from the two models and measured absorption coefficients are illustrated in Figures 21-24 for each sample.

The results illustrated in Figures 21-24 show that, the predicted values show good agreement with measured values of normal incidence absorption coefficients especially at frequencies where absorption peaks occur. General characteristics of the absorption curve are very similar, especially for the samples 1 and 2. Also, for samples 3 and 4, absorption characteristics are at resemblance. With the agreement between the measurements and predictions, it can be concluded that the general procedure defined up to now can be used for designing micro-perforated absorbers from Parabeam<sup>®</sup>.

As a general comparison between the analytical model and finite element model predictions: analytical model prediction results in under estimated normal incidence absorption coefficients and finite element model prediction tends to overestimate the absorption coefficients.

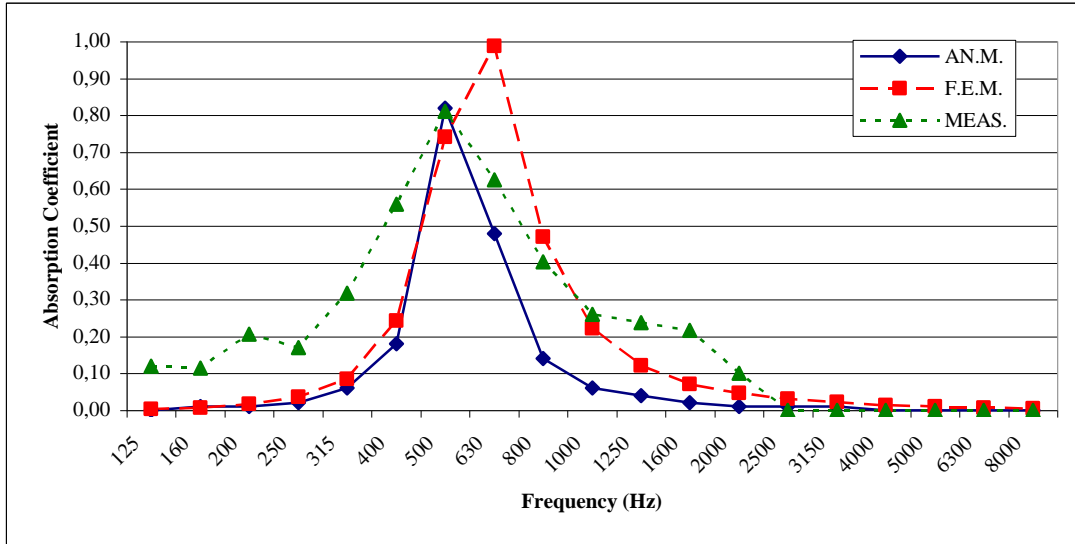


Figure 21. Results of predicted and measured normal incidence absorption coefficients for Sample 1: analytical model (blue-solid), finite element model (red-dashed), impedance tube measurements (green-dotted)

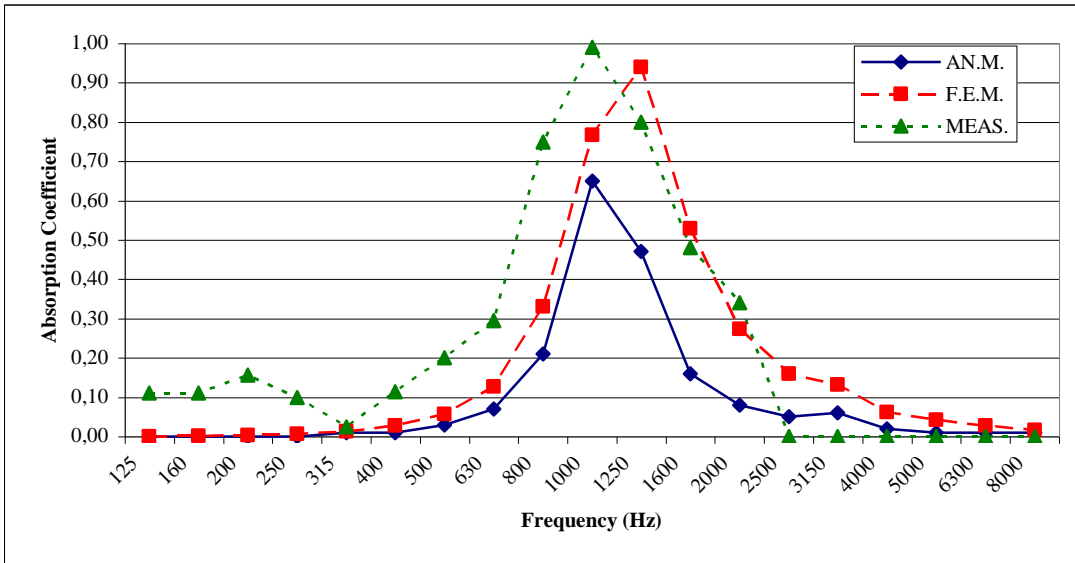


Figure 22. Results of predicted and measured normal incidence absorption coefficients for Sample 2: analytical model (blue-solid), finite element model (red-dashed), impedance tube measurements (green-dotted)

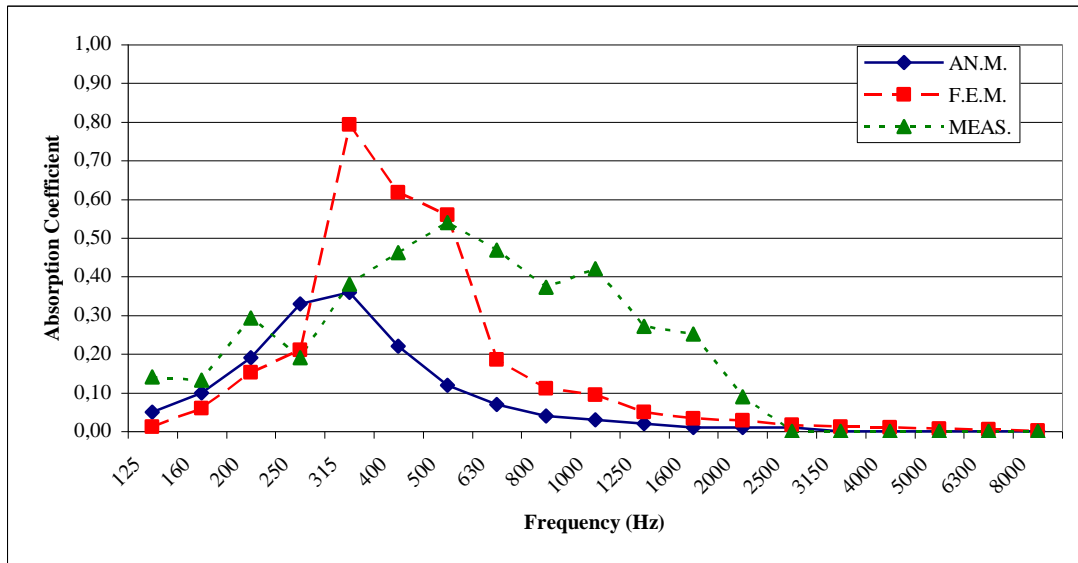


Figure 23. Results of predicted and measured normal incidence absorption coefficients for Sample 3: analytical model (blue-solid), finite element model (red-dashed), impedance tube measurements (green-dotted)

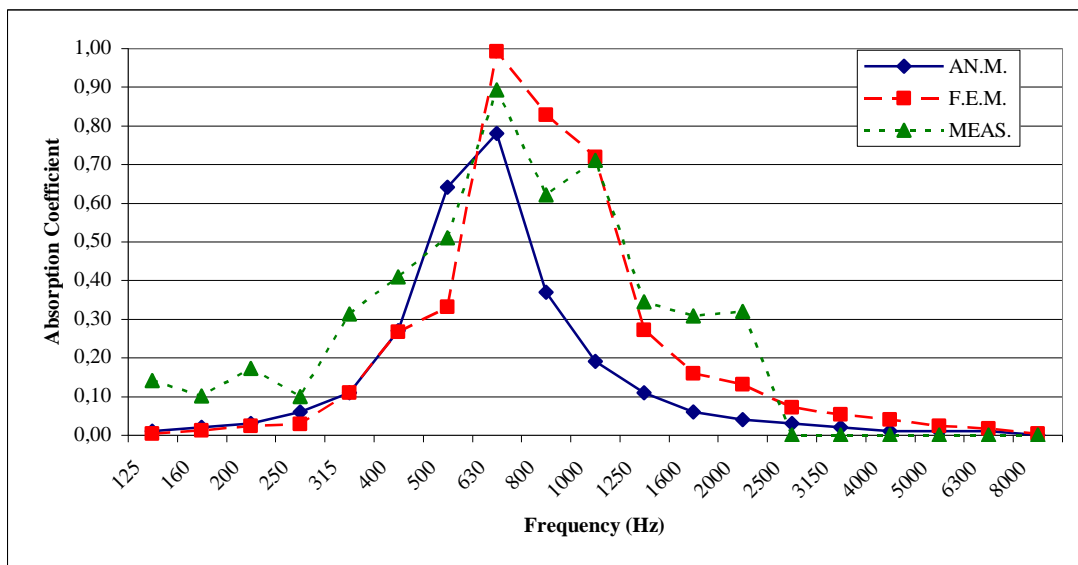


Figure 24. Results of predicted and measured normal incidence absorption coefficients for Sample 4: analytical model (blue-solid), finite element model (red-dashed), impedance tube measurements (green-dotted)

The resulting errors based on impedance tube measurements for each sample at the peak absorption frequencies are tolerable. Errors at frequencies other than peak absorption frequency are not too much significant because the absorption values at most of these frequencies are low. Even with the high percents of error present at these frequencies, this error is caused by differences around 0.05 in values of the absorption coefficient. Errors associated with frequencies where absorption peaks occur is especially low for finite element predictions.

As an example, for sample 1, whose peak absorption occurs at 500 Hz, the error based on impedance tube measurements is 7.4 % for analytical model and 8.4 % for finite element predictions at 500 Hz. Similarly, for sample 2, whose peak absorption occurs at 1000 Hz, the error based on impedance tube measurements is 34.3 % for analytical model and 22.4 % for finite element predictions at 500 Hz.

## **7.2 Optimization**

It is quite evident that, the analytical model developed is the quickest tool for the design of micro-perforated absorbers. For quick and effective design, analytical model can firstly be used by several runs and the absorption coefficient values obtained can be verified using finite element model and impedance tube measurements for a more accurate design. However, the analytical model is shown to predict underestimated absorption coefficients for four samples considered in the study.

For effective design of micro-perforated absorbers from Parabeam<sup>®</sup>, a spreadsheet is developed in MS EXCEL. The routine is used to optimize the absorption coefficient values by changing the absorber configuration.

The general design parameters for a single layer micro-perforated absorber with non-permeable, rigid perforated face (where structural vibrations of the perforated face does not have significant effects on absorption) are:

- Thickness of the perforated face

- Diameter of the holes
- Hole spacing (or hole pitch)
- Thickness of the air layer between the perforated face and rigid backing.

For the current absorber developed, the two parameters, thickness of the perforated face and the thickness of the fibrous layer or Parabeam<sup>®</sup> (or air layer) are constant, by the nature of the material.

The current design parameters and also the geometrical parameters that will be varied for optimization of the absorption characteristics of the micro-perforated absorber from Parabeam<sup>®</sup> are the diameter of the holes and the hole spacing. The diameter of holes is limited by means of manufacturing tools and techniques. Punching and hot drilling results in degradation of structure and poorly finished holes and surface. Drilling the holes by laser is also not possible. Among common manufacturing techniques, conventional drilling is the only way for the holes and by this technique with common tools used; diameter of the holes must be, at least, 0.5 mm.

The analytical model is employed for optimization by assignment of a linear objective function. The objective function for the optimization is defined as the sum of a linear combination of the absorption coefficient values at octave band center frequencies with different weightings assigned to each frequency. In the optimization, since there is no suggested weighing available in literature, weightings for each frequency are varied between 1 and 10 in the frequency range where the absorber is found as effective from the four samples. The optimized values for hole spacing and hole diameter are obtained by trial of several weightings assigned which are varied manually. It is also discovered that results of the optimization is not affected too much by these weightings. As seen from the results illustrated in previous pages, the hole spacing and hole diameter have limited effect on the absorption characteristics of absorber.

The optimization results in an absorber configuration with the diameter of holes being 0.8 mm and the hole spacing being 13 mm. The predicted results from

analytical model and finite element model and results of measurements are illustrated in the Figure 25.

The accuracy of prediction of the optimized absorber is very similar to predictions for samples. Predictions give good results at peak absorption frequencies.

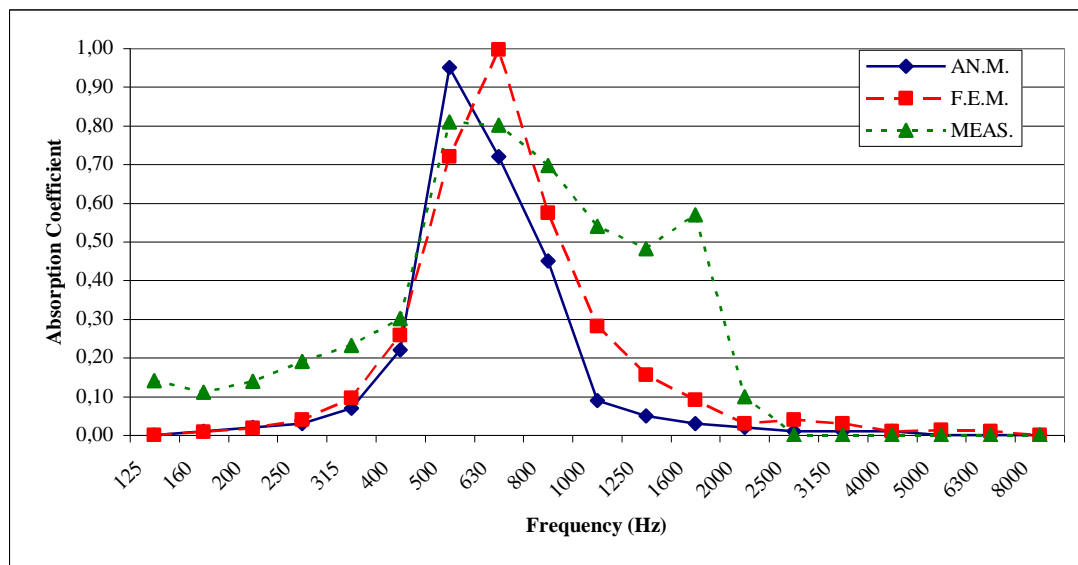


Figure 25. Results of predicted and measured normal incidence absorption coefficients for the optimized absorber: analytical model (blue-solid), finite element model (red-dashed), impedance tube measurements (green-dotted)

In general, accuracy of results obtained for peak absorption frequencies are better than other frequencies. Finite element and analytical model predictions differ especially between the frequencies 1000 Hz and 2000 Hz, where an unexpected good absorption performance is obtained. It is also clear that by the nature of Parabeam<sup>®</sup>, effective absorbers with peak absorption values at the frequencies 500 Hz and 1000 Hz can be designed.

## CHAPTER 8

### DISCUSSIONS AND CONCLUSIONS

Results obtained from analytical and finite element models and experimental results have described an integrated approach for prediction of normal incidence absorption coefficients of the micro-perforated absorber built from Parabeam<sup>®</sup>. The analytical model utilized in MATLAB<sup>®</sup>, the finite element solution obtained using MSC.ACTRAN and impedance tube measurements are employed for effective design and optimization of the absorber.

The results, discussions and conclusions of most significance are briefly summarized below:

1. The results obtained from analytical model, finite element model and impedance tube measurements generally show good agreement. As seen from the Figures 21 to 25, results obtained from finite element model give closer results to impedance tube measurements than results obtained from analytical model. It can also be concluded that, analytical model predictions give the safest values for design. Almost all values obtained from analytical model are smaller from those measured. The general character of the absorption curves fit to each other with an average error of 48.6 % for analytical model predictions and 34.4 for % for finite element model predictions. The error percentage is simply defined as the ratio of the difference between the predicted values (either analytical or finite element model prediction) and measured values to measured values. The absorption coefficient values below 0.4 are not taken into consideration for error analysis. These levels of error are somehow tolerable. Large amounts of error and frequency shift in peak absorption frequencies for

Sample 3 may possibly be caused by an unidentified coupling between fibers and micro-perforation. With the agreement between the results shown, it can be concluded that analytical model is a safe design tool for the micro-perforated absorber made from Parabeam<sup>®</sup>.

2. The absorption coefficients resulting from all three methods show that the micro-perforated absorber built from Parabeam<sup>®</sup> is effective in a relatively narrow frequency band covering at most 3 octaves with the current configuration.

3. The effect of the fibers in the middle layer of Parabeam<sup>®</sup> is seen by the calculated impedance values at the top of the fibers from the finite element model. With almost purely imaginary impedance values obtained, it is clear that presence of fibers do not considerably affect the resulting acoustic resistance of the layer. Purely imaginary impedance resembles the impedance and character of a common enclosed air layer with fibers modifying the imaginary parts of the impedance values. Even, with fibers not contributing to the acoustic resistance of the middle layer, they solve the important problem of supporting the micro-perforated layer, by backing it and joining it with the bottom layer in a natural way. By this, the micro-perforated absorber to be built just by simply drilling micro holes to a face of Parabeam<sup>®</sup> can be placed anywhere as an integral material without any supporting structure by simple mounting.

4. The analytical model developed offers a fast prediction tool by simply inputting the parameters of the micro-perforated absorber, as described in Chapter 4. The tool not only offers prediction for Parabeam<sup>®</sup>, necessary equations and parameters are defined in the tool for air and fibrous/porous absorber layers. Also, it is possible to predict the absorption coefficients of absorbers in the whole frequency range of interest other than prediction only in octave band frequencies, very quickly. (For this kind of prediction of Parabeam<sup>®</sup>, the impedance at the top of the fibers should also be evaluated for the whole frequency span.)

5. The results obtained from the finite element method also show good agreement with measurements. The complex geometry and distribution of the fibers makes both

modeling and later meshing the model very hard. So, the layer is modeled as closely possible to exact material geometrically. In the model, the distance between consecutive fibers are a bit larger than the exact distance. The impedance values obtained from the finite element model and the agreement between results show that, this fiber configuration does not result in boundary layer friction and resulting acoustic resistance. There is no doubt that the exact modeling will give better results but the model develop can be thought to be adequate for simulation of the fibers.

6. The sample size of 6 x 9.6 mm is chosen by consecutive finite element solution of samples of different sizes using augmentation of same pattern. Results are observed by increasing sample size step by step and it is found that after this size, there is no significant change in results. Hence, this size was chosen for all other finite element models built. Even with this small sample size, finite element solution for a single frequency of a sample takes around 30 minutes by use of a PC with 1.66 GHz Intel Core Duo processor and 1 GB of ram.

7. The measurements are performed on a standing wave tube method impedance tube setup which is relatively old. The required amplitudes are read from the digital screen of oscillator by naked eye, which may lead to errors. Also, the upper frequency limit of the impedance tube apparatus is around 2460 Hz so, the absorption coefficient values above 2000 Hz cannot be measured. The values are taken as zero and with the agreement observed between results from predictions and measurements at other frequencies; very low absorption coefficient values obtained from predictions can be accepted as resultant absorption coefficients above 2000 Hz.

8. An average constant absorption coefficient value around 0.15 is obtained for each sample including the optimized sample from the measurements at the frequencies up to 250 Hz. There is not much possibility to obtain such low frequency absorption. It can be anticipated that this result is due to Parabeam<sup>®</sup> itself. Such low frequency absorption can possibly be obtained by appropriate configuration for micro perforation with smaller plate thickness and smaller hole diameters but no such configuration exist. It can be concluded that that constant absorption coefficient

values are caused by the impedance tube apparatus, most possibly by the losses from the plastic walls of the tube itself.

9. In the optimization procedure it is clearly seen that an absorber covering a wider band is not too much possible by the nature of Parabeam<sup>®</sup>. As observed from existing literature, an effective wideband micro-perforated absorber requires smaller thickness of micro perforation layer and smaller hole diameters. These two values should also be close to each other. With thickness of the micro-perforated layer being 1 mm in Parabeam<sup>®</sup>, an effective wideband absorber configuration is not much possible. Trimming the plate to a smaller thickness seems to be a possible solution to this.

Future work on this subject should be concentrated on widening the effective absorption range of the absorber. Lowering the thickness of the face and the hole diameter is one possible solution. Multi-layer micro-perforated absorbers with micro-perforated layers with different configurations and separated by air spaces is another solution for this. It should be noted that, multi layer absorber assemblies including Parabeam<sup>®</sup> require further processes both for manufacturing and assembly of consecutive layers including air spaces. Also, using different types of porous, fibrous or any possible kind of absorber layers may also result in interesting absorption characteristics.

Further work should also focus on development of a double leaf micro-perforated absorber from Parabeam<sup>®</sup>, by additionally drilling holes to base plate of Parabeam<sup>®</sup> along with top plate. Both transmission loss and absorption characteristics should be investigated in this configuration.

Another future work should be concentrated on prediction and verification of random incidence absorption coefficients. With predictions of random incidence absorption coefficients, in situ performance of the absorber can be investigated in a more realistic way.

## REFERENCES

- [1] Parabeam Product Family Brochure, Parabeam 3D Glass Fabrics B.V.
- [2] D. Y. Maa, “Microperforated-panel wideband absorbers”, *Noise Control Engineering Journal*, Vol. 29, No. 3, pp. 77–84, 1987
- [3] D. Y. Maa, “Potential of microperforated panel absorber”, *Journal of Acoustical Society of America*, Vol. 104, No. 5, pp. 2861-2866, 1998
- [4] M. R. Stinson, E. A. G. Shaw, “Acoustic impedance of small circular orifices in thin plates”, *Journal of Acoustical Society of America*, Vol. 77, No. 6, pp. 2039-2042, 1985
- [5] C. Zwikker, C. W. Kosten, “Sound Absorbing Materials”, Elsevier Publishing Company, Inc., New York, 1949
- [6] J. Zou, Y. Shen, J. Yang and X. Qui, “A note on the prediction method of reverberation absorption coefficient of double layer micro-perforated membrane”, *Applied Acoustics*, Vol. 67, pp. 106-111, 2006
- [7] Z. Chongyun, H. Quibai, “A method for calculating the absorption coefficient of a multi-layer absorbent using the electro-acoustic analogy”, *Applied Acoustics*, Vol. 66, pp. 879-887, 2005
- [8] F. C. Lee and W. H. Chen, “Acoustic transmission analysis of multi-layer absorbers”, *Journal of Sound and Vibration*, Vol. 248, No. 4, pp. 621-934, 2001

- [9] M. A. Delany and E. N. Bazley, "Acoustic properties of fibrous absorbent materials", *Applied Acoustics*, Vol. 3, pp.105-116, 1970
- [10] J. Kang and H. V. Fuchs, "Predicting the absorption of open weave textiles and micro-perforated membranes backed by an airspace", *Journal of Sound and Vibration*, Vol. 220, pp. 905-920, 1999
- [11] D. Takahashi, "A new method for predicting the sound absorption of perforated absorber systems", *Applied Acoustics*, Vol. 51, No. 1, pp. 71-84, 1997
- [12] K. Sakagami, T. Uyama, M. Morimoto, M. Kiyama, "Prediction of the reverberation absorption coefficient of finite-size membrane absorbers", *Applied Acoustics*, Vol. 66, pp. 653–668, 2005
- [13] Y. Lee, E. W. M. Lee and C. F. Ng, "Sound absorption of a finite flexible micro-perforated panel backed by an air cavity", *Journal of Sound and Vibration*, Vol. 287, pp. 227-243, 2005
- [14] Y. Y. Lee, C. F. Ng, and C. K. Hui, "Study the panel and Helmholtz resonances of a micro-perforated absorber" 14th International Congress on Sound & Vibration, Cairns, Australia, July 2007
- [15] K. Sakagami, M. Morimoto and M. Yairi, "A note on the effect of vibration of a microperforated panel on its sound absorption characteristics", *Acoustical Science & Technology*, Vol. 26, No. 2, pp. 204-207, 2005
- [16] D. Takahashi and M. Tanaka, "Flexural vibration of perforated plates and porous elastic materials under acoustic loading", *Journal of Acoustical Society of America*, Vol. 112, No. 4, pp. 1456-1464, 2002
- [17] D.H. Leea, Y.P. Kwon, "Estimation of the absorption performance of multiple layer perforated panel systems by transfer matrix method", *Journal of Sound and Vibration*, Vol. 278, pp. 847–860, 2004

- [18] J. F. Alard and Y. Champoux, “New empirical equations for sound propagation in rigid frame fibrous materials”, *Journal of Acoustical Society of America*, Vol. 91, No. 6, pp. 3346-3353, 1992
- [19] K. V. Horoshenkov and K. Sakagami, “A method to calculate the acoustic response of a thin, baffled, simply supported poroelastic plate”, *Journal of Acoustical Society of America*, Vol. 110, No. 2, pp. 904-917, 2001
- [20] S. Sugie, J. Yoshimura and H. Ogawa, “Absorption characteristics of fibrous material covered with perforated facing and film”, *Acoustic Science & Technology*, Vol. 27, No. 2, pp. 87-96, 2006
- [21] I. Lee, A. Selamet and N. T. Huff, “Acoustic impedance of perforations in contact with fibrous material”, *Journal of Acoustical Society of America*, Vol. 119, No. 5, pp. 2785-2797, 2006
- [22] Z. Hong, L. Bo., H. Guangsu and H. Jia, “A novel composite sound absorber with recycled rubber particles”, *Journal of Sound and Vibration*, Vol. 304, pp. 400–406, 2007
- [23] N. Atalla and R. Panneton, “Acoustic absorption of macro-perforated porous materials”, *Journal of Sound and Vibration*, Vol. 243, No. 4, pp. 659-678, 2001
- [24] F. X. Bécot, L. Jaouen, E. Gourdon, “Modeling the absorption of non planar acoustic materials”, 19th International Congress on Acoustics Madrid, September 2007
- [25] K. Sakagami, M. Kiyama, M. Morimotoa, “Acoustic properties of double-leaf membranes with a permeable leaf on sound incidence side”, *Applied Acoustics*, Vol. 63, pp. 911–926, 2002

- [26] D. Takahashi K. Sakagami and M. Morimoto, “Acoustic properties of permeable membranes”, *Journal of Acoustical Society of America*, Vol. 99, No. 5, pp 3003-3009, 1996
- [27] O. Godbold, J. Kang, R. Soar, R. Buswell, “From MPA to Strategically Designed Absorbers Using Solid Freeform Fabrication Techniques”, 19th International Congress on Acoustics Madrid, September 2007
- [28] H. Chen, F. C. Lee and D. M. Chiang, “On the acoustic absorption of porous materials with different surface shapes and perforated plates”, *Journal of Sound and Vibration*, Vol. 237, No. 2, pp. 337-355, 2000
- [29] F. C. Lee, W. H. Chen, “On the acoustic absorption of multi-layer absorbers with different inner structures”, *Journal of Sound and Vibration*, Vol. 259, No. 4, pp. 761-777, 2003
- [30] A. Panteghini, F. Genna and E. Piana “Analysis of a perforated panel for the correction of low frequency resonances in medium size rooms”, *Applied Acoustics*, Vol. 68, pp. 1086–1103, 2007
- [31] M. C. Chiu, Y. C. Chang, L. J. Yeh and G. J. Lai, “Computer-aided design on a perforated single-layer absorber under space constraints”, *International Journal of Advanced Manufacturing Technology*, Vol. 32, pp. 537-546, 2006
- [32] Y. Shen, H. Wang, “Quick design for the micro-perforated sound absorber”, 19th International Congress on Acoustics Madrid, September 2007
- [33] J. Kang and H. V. Fuchs, “Effect of water-films on the absorption of membrane absorbers”, *Applied Acoustics*, Vol. 56, pp. 127-135, 1999
- [34] K. Sakagami, M. Morimoto and M. Yairi, “A note on the effect of vibration of a microperforated panel on its sound absorption characteristics”, *Acoustical Science & Technology*, Vol. 26, No. 2, pp. 204-207, 2005

- [35] K. Sakagami, M. Morimoto and W. Koike, “A numerical study of double-leaf microperforated panel absorbers”, *Applied Acoustics*, Vol. 67, pp. 609–619, 2006
- [36] K. Sakagami, T. Nakamori, M. Morimoto, M. Yairi, “Double-leaf microperforated panel space absorbers a revised theory and detailed analysis”, 19th International Congress on Acoustics Madrid, September 2007
- [37] M. Yairi, K. Sakagami, M. Morimoto, “Double leaf microperforated panel space absorbers an experimental study for further improvement”, 19th International Congress on Acoustics Madrid, September 2007
- [38] M. Toyoda, D. Takahashi, “Sound insulation characteristics of a micro-perforated panel with a subdivided air layer”, 19th International Congress on Acoustics Madrid, September 2007
- [39] K. Sakagami, Masayuki Morimoto, M. Yairi, A. Minemura, “A pilot study on improving the absorptivity of a thick microperforated panel absorber”, *Applied Acoustics*, Vol. 69, No. 2, 2008
- [40] M. I. Mide, “Dual-size MPP absorber with coupled air cavity”, 19th International Congress on Acoustics Madrid, September 2007
- [41] P. Cobo and M. Cuesta, “Hybrid passive-active absorption of a microperforated panel in free field conditions”, *Journal of Acoustical Society of America*, Vol. 121, No. 6, 2007
- [42] J. Pfretzschner, P. Cobo, F. Simon, M. Cuesta, A. Fernandez, “Hybrid passive-active absorption of broadband noise using MPPs”, *Applied Acoustics*, Vol. 67, pp. 62-73, 2006
- [43] Z. M. Zhang, X. T. Gu “The theoretical and application study on a double layer microperforated sound absorption structure”, *Journal of Sound and Vibration*, Vol. 215, No. 3, pp. 399-405, 1998

- [44] B. Fenech, G. M. Keith, and F. Jacobsen “The use of microperforated plates to attenuate cavity resonances”, *Journal of Acoustical Society of America*, Vol. 120, No. 4, pp. 1851-1858, 2007
- [45] D. Takahashi, “Sound transmission through single plates with absorptive facings”, *Journal of Acoustical Society of America*, Vol. 84, pp. 1453-1457, 1988
- [46] D. Takahashi, “Sound transmission through single plates with absorptive facings: Improved theory and experiment”, *Journal of Acoustical Society of America*, Vol. 88, No. 2, pp. 879-882, 1990
- [47] M. Toyoda and D. Takahashi, “Reduction of acoustic radiation by impedance control with a perforated absorber system”, *Journal of Sound and Vibration*, Vol. 286, pp. 601-614, 2005
- [48] I. D. Abrahams, “Sound radiation from a line forced perforated elastic sandwich panel”, *Journal of Acoustical Society of America*, Vol. 105, No. 6, pp. 3009-3020, 1999
- [49] T. J. Cox and P. D’Antonio, “Acoustic Absorbers and Diffusers: Theory, Design and Application”, Spon Press, Oxon, 2004
- [50] MSC.ACTRAN Manual, FFT Technologies, 2007
- [51] MSC.ACTRAN Lecture Notes: “Mechel’s Formula”
- [52] ISO 10534-2:1998: “Acoustics - Determination of sound absorption coefficient and impedance in impedance tubes - Part 1: Method using standing wave ratio”

## APPENDIX A

### MATLAB<sup>®</sup> CODE OF THE ANALYTICAL MODEL

```
function perforated(A)
f=[125 160 200 250 315 400 500 630 800 1000 1250 1600 2000 2500 3150 4000
5000 6300 8000] % definition of evaluated frequencies
ro=1.21 % density of air
c=340 % speed of sound in air
viscosity=1.85e-5 % viscosity of air
w=2*pi*f % angular frequency
kair=w/c % wave number of air
m=1 % indice for number of total layers
for v = 1:50
    if A(v,1)~=0
        m=m+1 %total number of layers
    else
        break
    end
end

for h = 1:m
    if A(h,1)==2 % PERFORATION
        t=A(h,2) %perforation thickness
        d=A(h,3) %perforaton diameter
        eta=A(h,4) % perforation ratio
        kd=d/2*sqrt(ro*w/viscosity) %perforate constant 1
        s=kd*sqrt(-j) %perforate constant 2
```

```

Zl=j*w*ro*t./(1-2*besselj(1,s)./(s.*besselj(0,s))) % impedance of short tube
Zl=Zl/eta+j*w*0.85*ro*d/eta+sqrt(2)*kd*viscosity/(d*eta) % impedance of
layer
Z=Z+Zl % impedance at the top of layer

elseif A(h,1)==3 % AIR
    t=A(h,2) % air thickness
    if (A(h-1,1)==1)
        Z=-i*ro*c*cot(kair*t) % impedance of air layer if backed by rigid wall
    else
        k=-j*kair % wave number in air layer
        Zl=ro*c % characteristic impedance of air layer
        Z=(-j.*Zl.*Z.*cot(k.*t)+Z.*Z)./(Zl-j.*Z.*cot(k.*t)) % transfer matrix equation
resulting in impedance at the top of the layer
        % Z=Zl*(Z*cosh(k*t)+Zl*sinh(k*t))/(Z*sinh(k*t)+Zl*cosh(k*t))
    end

elseif A(h,1)==4 % POROUS - FIBROUS ABSORBER
    t=A(h,2) % porous layer thickness
    Rf=A(h,3) % flow resistivity
    kp=w./c.*((0.189.*(ro.*f./Rf).^(-0.595))+i.*w./c.*(1+0.0978.*(ro.*f./Rf).^(-
0.7))) % wave number in porous layer
    Zl=ro.*c.*((1+0.057.*(ro.*f./Rf).^(-0.754))-i.*(0.087.*(ro.*f./Rf).^(-0.732)))
% characteristic impedance of porous layer
    if (A(h-1,1)==1)
        Z=Zl.*coth(kp.*t) % impedance of porous layer if backed by rigid wall
    else
        % Z=(-j.*Zl.*Z.*cot(kp*t)+Z.*Z)./(Zl-j.*Z.*cot(kp*t)) % transfer matrix
equation resulting in impedance at the top of the layer
        Z=Zl.*(Z.*cosh(kp*t)+Zl.*sinh(kp*t))./(Z.*sinh(kp*t)+Zl.*cosh(kp*t))
    end
end

```

```

elseif A(h,1)==5 %                FIBROUS LAYER OF PARABEAM
    Z=[-0.022-i.*11798.454, 0.0713-i.*9188.81, 0.049-i.*7335.53, -0.109-
i.*5857.352, 0.007-i.*4639.02, 0.0048-i.*3642.82, 0.001-i.*2900.705, 0.0017-
i.*2291.03, -0.002-i.*1786.24, 0.001-i.*1409.28, -0.003-i.*1100.88, 0.0007-
i.*823.30, 0.001-i.*614.278, 0-i.* 454.51, -0.006-i.*1440.94, 0-i.*110.466,
0+i.*54.10, -0.00011+i.*296.86, 0+i.*420.213]
    end
end

R=(Z-ro.*c)/(Z+ro.*c) % reflection coefficient
alfa=1-(abs(R)).^2 % normal incidence absorption values

hold on
semilogx(f,alfa,'b')
xlabel('f (Hz)')
ylabel('Absorption Coefficient')
axis([50 8000 0 1])
file1=fopen('output.txt', 'w')
fprintf(file1,'%0.2f \n',alfa)
fclose(file1)

```

## APPENDIX B

### FINITE ELEMENT THEORY OF MSC.ACTRAN MODAL BASIS

The propagation in a duct subjected to a uniform subsonic flow along z direction (Mach number M) can be described by the convected wave equation written in Cartesian coordinates (x, y, z) with  $\phi$  being the velocity potential and k is the wave number in air:

$$\frac{\partial^2 \phi}{\partial x^2} + \frac{\partial^2 \phi}{\partial y^2} + (1 - M^2) \frac{\partial^2 \phi}{\partial z^2} - 2jkM \frac{\partial \phi}{\partial z} + k^2 \phi = 0 \quad (\text{B.1})$$

The acoustic pressure and p and velocity vector v are given by:

$$p = -\rho_{air} c \left( jk\phi + M \frac{\partial \phi}{\partial z} \right) \quad (\text{B.2})$$

$$v = \nabla \phi \quad (\text{B.3})$$

where  $\rho_{air}$  and c are density of air and speed of sound in air respectively.

For the solution of the wave equation for the uniform flow case, Prandtl -Glauert transformation is applied. With the help of this transformation, reduction of the convected wave equation to the Helmholtz equation can be achieved.

Prandtl – Glauert transformation involves the change of variables as:

$$\begin{pmatrix} x \\ y \\ z \end{pmatrix} \rightarrow \begin{pmatrix} x' = x \\ y' = y \\ z' = \frac{z}{\beta} \end{pmatrix} \quad (\text{B.4})$$

where  $\beta$  is defined as:

$$\beta = \sqrt{1 - M^2} \quad (\text{B.5})$$

Also, if we select a variable  $\phi'$  as:

$$\phi' = \phi \cdot e^{-jk \frac{M}{\beta^2} z} \quad (\text{B.6})$$

Equation B.1 can be written as:

$$\Delta \phi' + \bar{k}^2 \phi' = 0 \quad (\text{B.7})$$

with  $\bar{k}$  being:

$$\bar{k} = \frac{k}{\beta} \quad (\text{B.8})$$

The solution to Equation B.7 can be obtained by using the transformation and then by separation by variables:

$$\phi'(x', y', z') = \sum_m \sum_n \sum_p F_m(x') F_n(y') F_p(z') \quad (\text{B.9})$$

The solution for  $\phi$  can be found by back transformation of B.4 as:

$$\phi(x, y, z) = \sum_m \sum_n \sum_p F_m(x) F_n(y) F_p\left(\frac{z}{\beta}\right) e^{-jk \frac{M}{\beta^2} z} \quad (\text{B.10})$$

This kind of procedure can be applied to any coordinate system including cylindrical, spherical or annular. More specifically, for a duct with a rectangular cross-section with transverse dimensions  $a$  and  $b$ , solution for  $\phi$  can be found as:

$$\phi(x, y, z) = \sum_{m=0}^{\infty} \sum_{n=0}^{\infty} \cos\left(\frac{m\pi x}{a}\right) \cos\left(\frac{n\pi y}{b}\right) \left( a_{mn}^+ e^{-jk_{zmn}^+ z} + a_{mn}^- e^{+jk_{zmn}^- z} \right) \quad (\text{B.11})$$

where  $m$  and  $n$  are modal orders along transverse directions  $x$  and  $y$  respectively while  $k_{zmn}^+$  and  $k_{zmn}^-$  are the longitudinal wavenumbers. A particular mode  $m, n$  for the solution can simply be written as:

$$\phi_{mn}(x, y, z) = A_{mn}^{\phi} \cos\left(\frac{m\pi x}{a}\right) \cos\left(\frac{n\pi y}{b}\right) e^{-ik_{zmn} z} \quad (\text{B.12})$$

This condition shows the form of a hard wall boundary condition in  $x = 0$ ,  $x = a$ ,  $y = 0$  and  $y = b$ ;

$$\left. \frac{\partial \phi}{\partial x} \right|_{x=0} = \left. \frac{\partial \phi}{\partial x} \right|_{x=a} = \left. \frac{\partial \phi}{\partial y} \right|_{y=0} = \left. \frac{\partial \phi}{\partial y} \right|_{y=b} = 0 \quad (\text{B.13})$$

The wave numbers in transversal directions can be introduced as:

$$k_{xm} = \frac{m\pi}{a} \quad (\text{B.14})$$

$$k_{yn} = \frac{n\pi}{b} \quad (\text{B.15})$$

With the help of these two wavenumbers,  $k_{zmn}^+$  and  $k_{zmn}^-$  can be obtained using the dispersion relation:

$$k_{zmn}^+ = \frac{-kM + \sqrt{k^2 - \beta^2(k_{xm}^2 + k_{yn}^2)}}{\beta^2} \quad (\text{B.16})$$

$$k_{zmn}^+ = \frac{+kM + \sqrt{k^2 - \beta^2(k_{xm}^2 + k_{ym}^2)}}{\beta^2} \quad (\text{B.17})$$

For obtaining the expression for average modal intensity, related to a specific mode  $(m,n)$ , the pressure  $p_{xm}$  and the particle velocity  $v_{xm}$  related to that mode should be specified. Modal pressure can be written as a function of velocity potential as:

$$p_{xm} = -\rho_0 c \left( ik\phi_{mn} + M \frac{\partial \phi_{mn}}{\partial z} \right) \quad (\text{B.18})$$

so that the modal pressure can be rewritten as a function of the wavenumbers:

$$p_{mn}(x, y, z) = A_{mn}^p \cos(k_{xm}x) \cos(k_{ym}y) e^{-jk_{zmn}z} \quad (\text{B.19})$$

The modal velocity vector can be obtained using:

$$v_{mn} = \nabla \phi_{mn} \quad (\text{B.20})$$

From this, the velocity component along the duct axis  $z$  can be found as:

$$v_{mnz} = \frac{\partial \phi_{mn}}{\partial z} = A_{mn}^\phi (-jk_{zmn}) \cos(k_{xm}x) \cos(k_{ym}y) e^{-jk_{zmn}z} \quad (\text{B.21})$$

where  $A_{mn}^p$  and  $A_{mn}^\phi$  are related to each other using the equation:

$$A_{mn}^\phi = \frac{A_{mn}^p}{-j\rho_0 c (k - Mk_{zmn})} \quad (\text{B.22})$$

The quadratic velocity  $|v_{mnz}|^2$  can be evaluated using Equation B.21 as:

$$|v_{mnz}|^2 = v_{mnz}^* \cdot v_{mnz} = |A_{mn}^\phi|^2 |k_{zmn}|^2 \cos^2(k_{xm}x) \cos^2(k_{ym}y) \quad (\text{B.23})$$

Similarly, quadratic pressure can also be evaluated as:

$$|p_{mn}|^2 = |A_{mn}^p|^2 \cos^2(k_{xm}x) \cos^2(k_{ym}y) \quad (\text{B.24})$$

The average modal intensity  $I_{mn}$  within the hard-walled rectangular duct can be obtained by integrating local intensity over the cross section at  $z = 0$  as:

$$I_{mn} = \frac{1}{ab} \int_0^a \int_0^b \frac{1}{2} \left( \text{Re}(p_{mn}^* v_{mz}) (1 + M^2 + M \left( \frac{|p_{mn}|^2}{\rho_0 c} + \rho_0 c |v_{mz}|^2 \right)) \right) dx dy \quad (\text{B.25})$$

where real part of  $p_{mn}^* v_{mz}$  can be found using Equations B.19 and B.21:

$$\text{Re}(p_{mn}^* v_{mz}) = \text{Re} \left( \frac{|A_{mn}^p|^2 k_{zmn} \cos^2(k_{xm}x) \cos^2(k_{ym}y)}{\rho_0 c (k - k_{zmn} M)} \right) \quad (\text{B.26})$$

The average modal intensity can be obtained by putting Equations B.23, B.24 and B.26 into Equation B.25 as:

$$I_{mn} = \frac{|A_{mn}^p|^2 N_{mn} ((1 + M^2) k \text{Re}(k_{zmn}) + M |k - M k_{zmn}|^2 - M^3 |k_{zmn}|^2)}{ab \rho_0 c |k - k_{zmn} M|^2} \quad (\text{B.27})$$

with  $N_{mn}$  being:

$$N_{mn} = \frac{1}{2} \int_0^a \int_0^b \cos^2(k_{xm}x) \cos^2(k_{ym}y) dx dy \quad (\text{B.28})$$